13

Applications of Optical Fibers to Spectroscopy: Detection of High Explosives and Other Threat Chemicals

Natalie Gaensbauer[1], Madeline Wrable-Rose[1], Gabriel Nieves-Colón[2], Migdalia Hidalgo-Santiago[2], Michael Ramírez[2], William Ortiz[2], Oliva M. Primera-Pedrozo[2], Yahn C. Pacheco-Londoño[2], Leonardo C. Pacheco-Londoño[2] and Samuel P. Hernandez-Rivera[2]

ALERT DHS Center of Excellence for Explosives

[1]Northeastern University, Boston, MA,

[2]Department of Chemistry, University of Puerto Rico, Mayagüez,

[1]USA

[2]Puerto Rico

1. Introduction

In the last decades, research worldwide in areas of national defense and homeland security has focused on the search for new technologies for the detection and characterization of explosives, chemical and biological threats (CBT) and narcotics in different environments and scenarios. In the case of *in situ* field detection of explosives, the technique generally used is ion mobility spectrometry (IMS). The major advantages of IMS are its sensitivity in the picogram range, its continuous real time monitoring capability, reasonable price due to instrumental simplicity and ease of automation (Steinfeld and Wormhoudt, 1998). However, in general terms, IMS has a limited linear range and cannot be used for quantitative analysis. Also, analyte and background responses exhibit variations that occur with different reactive gas compositions and sample compositions. Moreover, it is relatively easy to overload an IMS. Therefore, sample mass and size must be limited.

Optical spectroscopy is routinely used for the measurement of many different species at trace levels. However, optical spectroscopy has not been extensively applied in the highly energetic materials (HEM) detection arena. This is due, in part, to physical constraints such as low vapor pressure, limited sample size, concealment, interferences and in part, to the spectroscopic characteristics of the compounds themselves (Steinfeld and Wormhoudt, 1998). Spectroscopic techniques have the potential to provide the best selectivity for explosives and offer an information-rich fingerprint that allows for near unambiguous identification. In the 1990's, direct detection by infrared absorption spectroscopy was not possible because of the limited sensitivity of this method. In addition, the test materials had to be placed physically within the spectrometer's sample compartment for measurement. The production of optical fibers cables (OFCs) that transmit in the mid-IR range made possible the development of a range of spectroscopic probes for *in situ* analysis (Melling and

Shelley, 2002); (Mehta et al., 2002). FTIR spectroscopy can now be effectively used outside the confinement of the sample compartment, making it available for field work. The establishment of RAIRS as an active area in the trace detection of chemicals is the result of a combination of high extinction coefficients in the MIR and the optical advantages of working at the grazing angle (Umemura, 2002). By combining a grazing angle head or probe (GAP) with a OFC that transmits in the MIR, the instrumentation becomes a platform for developing methodologies for real time, remotely sensed, *in situ* analysis (Mehta et al, 2002). GAP-FTIR operating in RAIRS mode with a sensing probe coupled to fiber optics has been used for the detection of active pharmaceutical ingredients (APIs) on metals (Mehta et al, 2003) and on glass surfaces (Hamilton et al., 2005). In these reports, combined teams from academia and the private sector demonstrated that the technique is an excellent alternative for the validation of cleanliness of metal walls of pharmaceutical reactors. Low limits of detection (LOD) ranging from 10 to 50 ng/cm^2 of single API were achieved (Mehta et al, 2003). In addition, the methodology was applied to quantify APIs in mixtures and was demonstrated to not depend solely on the reflective properties of metallic surfaces, making detection on other surfaces such as glass and plastic surfaces viable (Person et al., 2007). These characteristics of the methodology offer clear advantages over the traditional, time consuming, laborious and operator driven, swab-based HPLC method of analysis routinely used by the pharmaceutical industry in the validation of the cleanliness of batch reactors and other vessels and pipes.

Over the last ten years our group has dedicated many of its research efforts to the development and use of coupling optical fibers (OF) to spectroscopic instrumentation for applications in CBT and explosives detection: from near field close to the sample to far field at sample to detector distances over 100 m. From transmitting the excitation source energy to collecting the sample emitted/scattered energy from the ultraviolet (UV) to the mid-infrared (MIR) regions of the electromagnetic spectrum, optical fibers have led the way to doing experiments outside the traditional sample compartments, thus taking the experiments to the sample rather than the sample to the instrument. In this chapter, three applications in which optical fibers play the central role of interfacing the samples with the sensors are reviewed. First, MIR transmitting optical fibers used to couple an FTIR interferometer to a grazing angle probe and measure the reflectance/absorption IR (RAIS) spectra of highly energetic materials (HEM) in neat form, in mixtures of HEM and in quantification and discrimination experiments. In the second application, bundles of optical fibers and single strands of fibers were use to guide laser beams to act as Raman excitation sources. Another set of fibers were used to collect the scattered Raman signal to the guide it to the entrance slit/plane of a high throughput optical spectrometer. In the third application discussed, optical fibers were used to couple visible and UV reflective telescopes to imaging spectrometers in order to implement a remote Raman system for standoff detection to 140 m of hazardous chemicals.

2. Optical fiber coupled grazing angle probe reflectance-absorption infrared spectroscopy

The analysis of traces of solid phase highly energetic materials (HEM) deposited onto substrates is essential in homeland security and national defense applications (Gillen et al, 2004). Moreover, the preparation of HEM standards is critical during system detection design for field applications and post-delivery instrument operation validation (MacCrehan, 2004). The practical development of high-quality solid-on-solid standards depends on the material

type, on the physical properties of the deposited analyte, such as its vapor pressure and solubility in an appropriate solvent, on HEM adhesion forces to the test surface, on temperature, on the solvents used for mass transfer and on the sample preparation method. Several analytical techniques have been used to ensure reliable and reproducible *in situ* trace HEM detection. Among these techniques, ion mobility spectrometry (IMS) (Hernandez et at., 2004; Hallowell, 2001; Ewing et al., 2001; Phares et al., 2000), secondary ion mass spectrometry: SIMS (Gillen et al., 2004) and optical fiber coupled grazing angle probe/Fourier transform reflection absorption infrared spectroscopy: OFC-GAP/FT-RAIRS (Pacheco-Londoño et al., 2007; Primera-Pedrozo el at., 2008; Primera-Pedrozo et al., 2009) have been used the most frequently. In the first two techniques, chemical analysis takes place after sample collection. This is typically used for handbags and carry-on luggage detection in airports (Ewing et al., 2001). In OFC-RAIRS, the mid IR (MIR) beam is directly focused on the sample area, and the measurements are done *in situ* without sample consumption or destruction (Primera-Pedrozo el at., 2008). Remote detection using remote infrared spectroscopy (RIRS) and remote Raman spectroscopy (RRS) systems have become important for detecting highly energetic materials as well as their formulations and mixtures on surfaces (Pacheco-Londoño et al., 2009). Thus, in the development of new techniques and instrumentation for trace detection, the incorporation of methodologies for production of high-quality samples and standards is required. For proper functioning of sensors, reliable standards are essential. Calibration curves can then be generated to quantify known analytes, sensors can be trained with standards to detect samples of unknown identity with chemical/physical properties similar to compounds in the data base and thus detection methods can be significantly enhanced. The applications of these specially prepared samples include use in experiments that require fine control of the distribution of loadings of analytes on surfaces. Another important application is in the establishment of reliable standards that may support an instrument response validation program.

The sample analysis setup is schematically presented in Fig. 1. A Remspec MIR grazing angle probe was used to collect the spectra. The grazing-angle head uses carefully aligned mirrors to deliver the beam to the sample surface at the grazing angle (approximately 80° from normal), to collect the reflected beam, and to return it to a detector (liquid nitrogen cooled MCT detector).

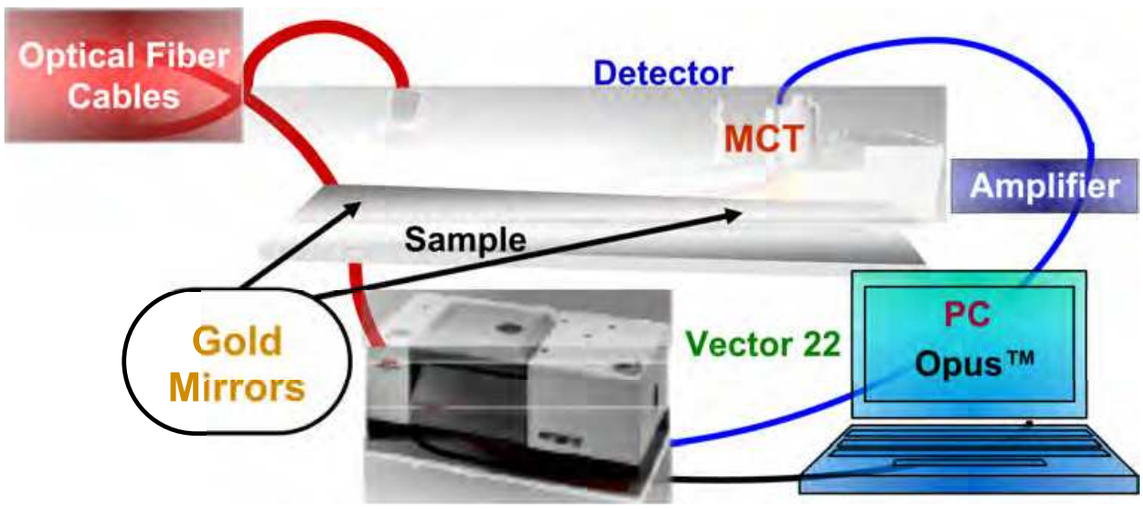

Fig. 1. Experimental setup for Fiber Optic Coupled-Grazing Angle Probe FTIR.

The signal is delivered from the spectrometer to the head by IR transmitting optical fiber cables. The grazing angle accessory is connected to the external beam port of the Bruker Vector 22 spectrometer by a 1.5 m, 19–fiber chalcogenide glass optical bundle in the As-Se-Te system, which transmits throughout the MIR with the exception of a strong H-Se absorbance band at 2200 cm^{-1}. The IR footprint produced by the grazing angle probe is elliptical with the intensity decaying from the middle towards the edges. The specially configured head illuminates a large spot on the sample surface. The spot is an ellipse 1 inch by six inches that is defined by a Gaussian distribution with a center spot about 1/8 inch by an inch. Electric signal from the MCT is delivered to the FTIR using an amplifier.

Sample smearing (Soto-Feliciano et al., 2006; Primera-Pedrozo, 2007; Primera-Pedrozo el at., 2008; Primera-Pedrozo et al., 2009) aerosol spray deposition, thermal inkjet deposition (Primera-Pedrozo et al, 2005; Wrable et al. 2010), deposition by rotary evaporation (MacCrehan, 2009), and direct transfer deposition using micropipettes (Primera-Pedrozo, 2005) have been reported previously as methods for sample and standards preparation on metals, silica, glass and plastic surfaces. Also, trinitrotoluene (TNT) was deposited on cloth and planar surfaces with post removal by air jets. The results proved that the particles that were less efficiently removed from the polycarbonate surface (Fletcher et al, 2008). Stickiness constitutes another method for producing plastic explosives deposits (Heimerl, 1999). A standard deposit on fibrous substrates method was developed by Phares and collaborators (Phares et al, 2000), in which the explosive suspension is first transferred to the Teflon with post drying. Then, the dried explosive deposit is pressed onto the tested substrate and mechanically transferring the sample without the associated liquid.

Piezoelectric and bubble-jet printing technologies have been used for microfabrication of biological samples with a rapid preparation of a large number of printed arrays at extremely low cost (Gillen et al. 2004). Both technologies have enabled deposition of femtomoles of analytes at an inkjet printer dot. These results make sample printing technologies excellent means for trace hazardous chemicals samples and standard manufacture. Thermal inkjet (TIJ) printers offer the advantages of being easy to wash and load and transfer of analytes using small amounts of sample (~ 20 μL). However, TIJ would be inappropriate for delivery of proteins on account of possible denaturation caused by exposure to a high temperature gradient. Inkjet printers can be used to fabricate microarrays containing biological materials (proteins, enzymes, etc). Thermal inkjet printers offer advantages compared to piezoelectric ones because they are easier to wash and reload and have the capability of depositing small volume samples. However, piezoelectric inkjet are preferred for protein and other biological molecules deposition because of heat stimulated denaturalization problems (Allain et al., 2004). In TIJ printing, a thin film resistor superheats less than 0.5% of the fluid in the chamber to form a gas bubble. This bubble rapidly expands (in less than 10 μs) and forces a drop to be ejected through a very small orifice (Beeson and Skip, 2000). The loading concentration of the sample on the surface can be controlled by varying parameters, such as the number of passes, the dispensing frequency, the applied energy and the pen architecture. Precise delivery of a known number of droplets with known mass and concentration is achieved. Also, by proper selection of the dispensing solution concentration, only one solution is required to dispense a broad range of surface concentrations, avoiding the preparation of several dilutions that could lead to analytical errors. In previous work, it was demonstrated that TIJ technology can be used for depositing 2,4,6-trinitrotoluene (TNT) and cyclotrimethylenetrinitramine (RDX) onto stainless steel surfaces, and TIJ-based deposition has been shown to be a superior method for further

detection using OFC-GAP/FT-RAIRS (Primera-Pedrozo et al., 2005). Visualization of deposits, using optical microscopy images, showed that there was a close dependence between the number of passes and the crystallization of the explosives on the surface. Even at a low (1.25 μg/cm^2) loading concentration, the surface was practically covered by crystals. Below this surface concentration, the formation of a metastable form of TNT was observed (Primera-Pedrozo et al., 2005).

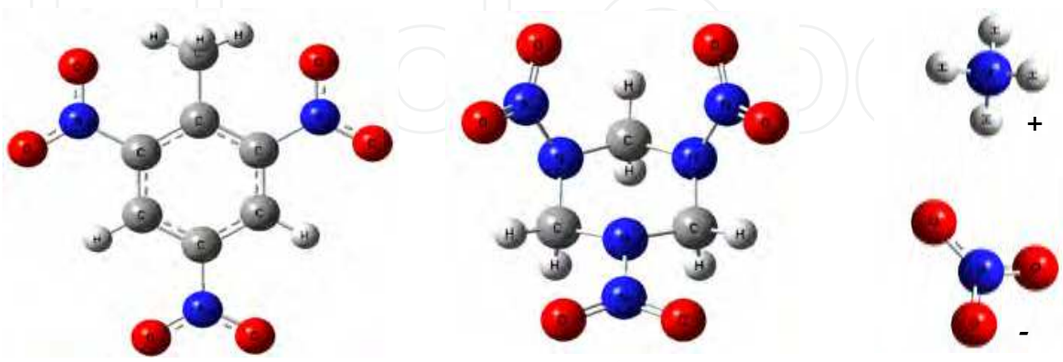

a b c

Fig. 2. Chemical structures of some of the highly energetic materials studied in OGC-GAP-RAIS experiments. (a) TNT; (b) RDX; (c) AN.

As demonstrated by Thundat and co-workers (Van Neste et al., 2009), the residence time of an analyte on a substrate depends on the surface energies, on the analyte-surface interaction forces and on the physical properties of the analyte deposited on the surface. Highly energetic materials, such RDX and PETN, take days to months to desorb from the surface. Thus, the physical properties of the deposited analytes and the substrate characteristics, such as vapor pressure and analyte-surface interactions, influence the preparation schemes of samples and standards. This report presents a broad view, from start to completion, of two schemes that can be used to establish efficient, reproducible and representative methodologies for preparing samples and standards of common contamination compounds. In this research, the following three HEMs were selected for the experiments: TNT, RDX and ammonium nitrate. Their chemical structures are shown in Fig. 2. Through the testing of various variables from materials to methods, a tailored approach will be apparent. This paper follows the timeline in which the experiments were performed, allowing the reader to easily follow why and how certain materials (solvents) and methods were modified based on the deposition characteristics desired. Each HEM studied required a unique mixture of solvents to prepare the optimum solutions for TIJ dispensing. The solvents used were all of HPLC grade and included methanol (MeOH, CH_3OH), acetonitrile (ACN, CH_3CN) and isopropyl alcohol, (IPA, $(CH_3)_2CHOH$)). These solvents were purchased from Fisher Scientific International. Distilled, deionized water was purified by reverse osmosis, followed by deionization and filtration through four stages of cartridges to remove organic and inorganic impurities and by exposure to far UV light to remove bacterial impurities (Nanopure Diamond, Barnstead, Thermo-Fisher Scientific, Inc., Waltham, MA).

A thermal inkjet (TIJ) X-Y-Z dispenser, model IIS-300S manufactured by ImTech, Inc. (Corvallis, OR), was used for printing the HEM onto the target surfaces. To begin the experiment, a bitmap (.bmp) image file of the desired design (1, 2 or 3 blocks) was chosen and loaded. The user-coordinates (print zone coordinate system) were as follows: x = 3.5 in,

y = 10 in. and z = 0.7 in. For the print head commands, the following settings were used: fire pulse = 2 μsec, warm pulse = 0.5 μsec, dead pulse = 0 μsec, voltage = 0 volts and the maximum frequency was 12 kHz. The IIS acceleration was as follows: x = 100 in/sec^2, y =100 in/sec^2 and z = 100 in/sec^2. The velocity was x = 10 in/sec, y=10 in/sec, z =10 in/sec and the IIS cap location was x = 1.90 in, y = 1.83 in, and z = 1.30 in. The solutions were dispensed using zero-dot spacing script (space between drops using HP inkjet) at a printing resolution of 600 dots per inch (dpi). Once the above specifications were set, the bitmap image was loaded and selected to print on the TIJ dispenser. The total printer area per substrate ("chip") was 1.0 cm × 0.8 cm (area = 0.8 cm^2). The bitmap images had three 0.8 cm^2 chips to be deposited per image, allowing 3 substrates to be printed at the same time. The total dispensing time for the surface area of 0.8 cm^2 was 14 s for a total of 56 s for three substrates. To allow enough drying time, a waiting period of 60 s was employed between printing passes. This waiting period was particularly important for high loading substrates that involved many passes. To carry out shelf life experiments, FOC-GAP/FT-RAIRS was used as a non destructive technique during a period of 15 hr. Details of the setup have been described previously (Primera et al. 2009).The most intense peak of the IR spectrum for each HEM was selected for the kinetics studies. In the case of RDX, the experiments were performed over one year. The experimental conditions were co-addition of 64 scans, 4 cm^{-1} resolution and a spectral range of 900–4,000 wavenumbers (cm^{-1}). In terms of consecutive measurements, the repeat setting was 100 times, and the delay between measurements was 100 s. Background spectra from clean test substrates were acquired using the same instrumental conditions as the sample spectra prior to each sample measurement session. All spectra were recorded in reflectance mode to facilitate data processing. To compare the influence of the surface type on the shelf life, experiments were performed on gold-on-silicon, glass, and stainless steel (SS) plates.

White light images of samples were acquired in order to maintain a record of the information concerning the loading surface distributions. This allowed comparisons between the two sample preparation methods and between the solvent mixtures used. An Olympus America, Inc. (Center Valley, PA) model BH2-UMA high resolution optical microscope designed for mineralogy studies and equipped with 10-250× magnification and a 6.0 MB PAX-Cam image capturing CCD camera controlled by the PAX-it!™ Software (Midwest Information Systems, Inc., Villa Park, IL) was used to capture white light images (micrographs) of the substrates with HEM loadings on them. Most of the images captured were taken with a 10× objective, but some micrographs required the use of infinity-corrected ultra long working distance Olympus objectives of 100× and 250× magnification. Nine images per sample were obtained by dividing the CCD chip into three rows and three columns.

For chemical analysis of the surface loadings of RDX and TNT, a model 1100 high performance liquid chromatograph (HPLC) from Agilent Technologies (Santa Clara, CA) equipped with a C-18 column (platinum, 100 A, 5 μm, 150 mm x 4.6 mm, Eclipse XDB Alltech), and a variable wavelength detector was used. The HPLC conditions employed were a flow of 1.0 mL/min, a stop time of 5 min and 3 min for TNT and RDX, respectively, a solvent mixture of 50% water and 50% methanol and a pressure limit of 400 bar. The chromatographic column was operated at 40 °C. Other conditions included a detector wavelength of 224 nm and 254 nm for TNT and RDX, respectively, with a pump time of 5 min, a peak width (response time) of less than 0.1 min, post time = off and an analysis time of 5 min. A model 732 IC ion chromatograph (Metrohm, Riverview, FL) was used for surface

loading analysis of AN. IC conditions included a retention time of 3.94 min, a mobile phase of 0.1 mM L-tartaric acid and 0.1 mM picolinic acid, an injection volume of 10 μL and a flow rate of 1 mL/min. Experiments were performed in cationic mode, and ammonium cations were detected.

The two methods tested for preparation of homogeneous samples and standards of solids/traces deposited onto surfaces were sample smearing (Primera-Pedrozo et al., 2008) and TIJ sample delivery (Primera-Pedrozo et al., 2005). Both methods were compared in the study. Two important parameters for dispensing analytes using TIJ are the solvent viscosity and surface tension. The value of the solvent viscosity must be between 2 and 6 x 10^{-2} g·cm^{-1}·s^{-1} (centipoises, cp), whereas the surface tension of the solution must be between 30 and 40 mN/m. IPA has a high viscosity compared to methanol and acetonitrile (2.8 cp), resulting in the formation of uniform spherical deposits (Van Neste et al., 2009). However, due the slight solubility of TNT and RDX in methanol and IPA, it was necessary first to dissolve them in acetonitrile and then to prepare a mixture of methanol and 2-propanol in order to have the adequate viscosity to dispense. The composition of the solvent was 10% acetonitrile, 20% methanol and 70% isopropanol. The use of 100% IPA as the solvent results in the formation of non-uniform droplets on silicon wafer surface and spread-out is observed. AN is highly soluble in water, and this constitutes a problem while dispensing. Thus, for the preparation of AN solutions, a small amount of the reagent was added to 3 mL of methanol and heated to 35°C until dissolved. This mixture was then transferred to a flask, and the vial was rinsed three times and transfer to the flask with IPA. The solvent ratio was changed until uniform, spherical deposits were found on the substrate images. Once the solutions were prepared, the analytes were deposited onto gold-on-silicon, glass or stainless steel substrates. The latter two substrates were used for comparison and as a means of obtaining information on analyte-substrate interactions. HEM solutions were prepared as explained in the previous section and, using a syringe, were transferred into one of the printer cartridges that was then used to print directly onto the substrates studied using the TIJ dispenser (Fig. 3). Low concentrations were used to avoid HEM nucleation and subsequent crystallization in the jet nozzles.

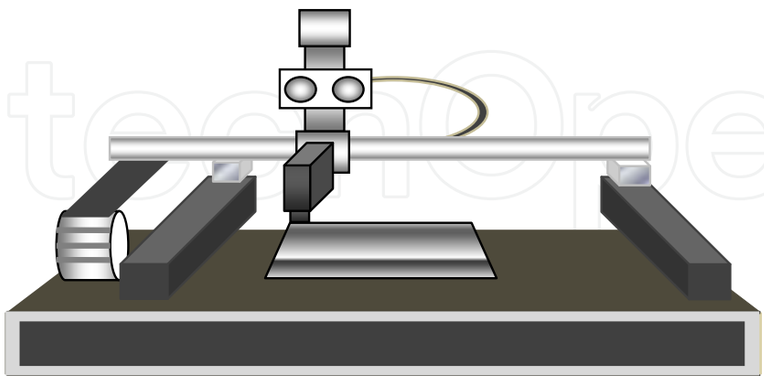

Fig. 3. Deposition method: thermal inkjet printer used for sample dispensing.

To obtain higher surface concentrations as 20-50 μg/cm², several print layers of solutions (passes) were applied. The cartridges were filled completely with 40 mL of HEM solution and then sealed shut with a small glass bead secured in place using adhesive tape. A

vacuum was then applied to the nozzle of the cartridge to ensure that the solution was ready to dispense. The cartridge was then placed in the printer head, and a personal computer (PC) was used to control the deposition program for dispensing by TIJ printing. Before dispensing by TIJ, a bitmap (*.bmp) image was required to determine precisely where to place the substrates. An MS Word™ (Microsoft Corporation, Redmond, WA) file was used to scale the target boxes until the dimensions matched those of the substrate. A width of 2.25 in and height of 2.00 in was found to produce an image that is 1.0 cm × 0.8 cm. Three samples were printed at one time (Fig. 4). These small squares were printed out in black to clearly show where the surfaces needed to be placed to ensure proper deposition.

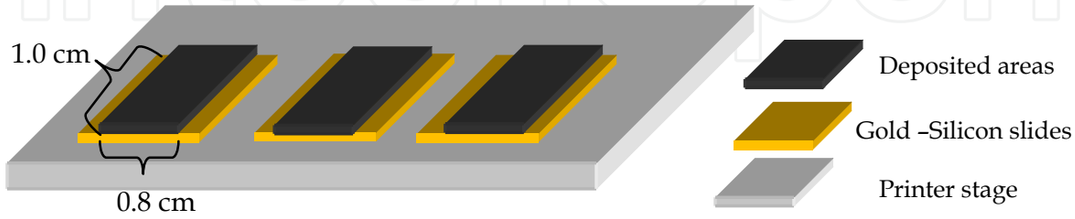

Fig. 4. Substrate deposition area for TIJ dispensing. Surface coverage was not complete, leaving 1 mm of surface uncoated on two sides for handling purposes.

The HEM loadings or surface concentrations (μg/cm²) deposited by TIJ or smearing were determined by HPLC or IC. To determine the total mass deposited onto the substrates, the latter were rinsed with an appropriate solvent and volume in which the HEM were highly soluble. Acetonitrile was used for rinsing RDX and TNT, but water was used for rinsing AN samples due to the high solubility of this HEM in water. Rinsing is the first and most critical step for determining how much explosive was originally deposited using both deposition methods. The substrates were printed onto an area of 0.8 cm × 1.0 cm, with 0.1 cm left free (Fig. 4) on each side to enable handling the substrate. To ensure that the analyte was rinsed entirely from the surface with as little loss as possible, tweezers were used to clamp the substrates by their corners, and a Pasteur pipette was used to rinse the substrate with the appropriate solvents. Care was taken to ensure that as much analyte as possible was removed. Once completed, the rinses were collected, transferred to small 1.0-mL vials, stirred to ensure uniform concentrations and analyzed for total mass collected using HPLC or IC. In the case of smeared samples, the total mass recovered was converted to percent recovery; however, in the case of TIJ deposition, this was not possible because the initial mass deposited was not readily known.

TIJ technology offers several advantages to smearing deposition. The method is less subject to human errors and provides more uniform target surface coverage. Moreover, the surface loading concentration can be varied by changing the numbers of passes delivered to the sample, the dispensing frequency, the applied energy and the dispensing pen architecture. Also, the method includes precise delivery of a number of droplets with well-characterized mass and concentration. Furthermore, only one solution is required, avoiding the need for serial dilutions that can increase the analytical errors caused by human intervention.

To ensure the feasibility of the method, the prepared dispensing solutions were also run in HPLC or IC to determine their exact concentration. Table 1 shows the results of the calibration curves used for determining the concentration of the HEM studied using HPLC or IC. RDX and TNT calibration curves were prepared using acetonitrile as the solvent,

while ultra high purity water was used for AN. Limits of detection (LOD) and limits of quantification (LOQ) for TNT and RDX using HPLC analysis and for AN using IC analysis are also reported. TNT had the lowest LOD and LOQ compared to RDX and AN. The exactly concentration of HEM solutions was also determined by HPLC or IC. The concentrations of these HEM solutions transferred to the ink cartridge were higher than the concentrations in the calibration curves (See Table 1), and thus it was necessary to prepare 1:10 (v/v) dilutions in acetonitrile to ensure the data fell into the proper concentration range.

HEM	Concentration range (ppm)	Method of analysis	R^2	LOD (ppm)	LOQ (ppm)	Significance F-value
TNT	0.1-1.5	HPLC	0.9990	0.05	0.15	$1.30x10^{-05}$
RDX	0.1-1.5	HPLC	0.9978	0.07	0.23	$4.43x10^{-05}$
AN	1.0-5.0	IC	0.9601	0.2	0.6	$3.25x10^{-06}$

Table 1. HPLC and IC calibration curve results for the highly energetic materials (HEM) studied.

A different solvent was used for the rinsing step of each HEM on account of their distinct physical properties. Many factors had to be taken into account such as HEM-solvent affinity (in terms of solubility), deposition methodology and HEM vapor pressure. The first step consisted of finding the right solvent for each HEM. TNT and RDX were soluble in methanol, but AN was soluble in water. The inorganic AN is a highly hygroscopic chemical, and it was difficult to avoid the absorption of water during the preparation of standards. To remove as much water as possible, AN was dried at room temperature in a vacuum oven and maintained in a desiccator for 24 hr prior to use. The solubility of TNT and RDX is high in acetonitrile and low in isopropanol. According to Primera-Pedrozo and co-workers, using methanol as the solvent for sample smearing gave the most uniform surface concentrations as determined by micro-FTIR surface analysis (Primera-Pedrozo et al., 2009). For TNT and RDX, a solvent mixture of 10% ACN, 20% MeOH and 70% IPA was used, whereas a mixture of 12% MeOH and 88% IPA was used in the case of AN.

The second step of the methodology was to find a solvent mixture compatible with each deposition method. Smearing requires a solution that can be easily spread over the substrate and dries quickly in order to achieve a uniform coverage and surface concentration. In addition, the size of the substrate where the deposition takes places influences the distribution and the readiness of the smearing process. When the size of the substrate is relatively large (> 10 cm^2), it is very easy to dispense the mixture containing the analyte with the Teflon applicator, resulting in a uniform surface coverage (Fierro-Mercado et al., 2010). Another parameter that plays an important role in the nature of the coverage of the substrate is analyte-surface interactions, and this effect will be discussed later. TIJ deposition requires the use of a moderately viscous solution for high quality printing. Thus, the solvent solutions used were tailored to each specific deposition method. Depending on the speed of drying of the solution containing the dispensed analyte, the mix was modified with a higher or lower vapor pressure adsolvent. If the solution took too long to dry, then the percentage of MeOH in the solvent was increased. It was found that HEMs studied were soluble in methanol. The high vapor pressure of MeOH resulted in quick evaporation and uniform

surface loading (Primera-Pedrozo et al., 2009). However, if the solvent mix required higher viscosity, then the percentage of IPA was increased to compensate for the lower viscosity of the adsolvent added. These modifications to the solvent mix tailored the vapor pressure and physical characteristics of the mix as well as the deposition characteristics of the HEMs studied.

Fig. 5 contains white light micrographs of RDX deposits on gold coated silicon substrates obtained after a single thermal inkjet pass. The dispensing experiments were performed using an 812 ppm RDX stock solution in 10% ACN, 20% MeOH and 70% IPA. Figure 5a shows that the central portion of the substrate is covered by a nearly uniform distribution of RDX deposits. The micrographs of the borders (Figure 5b, inner part of border) showed the presence of small RDX crystals, while the micrograph included in Figure 5c (outer part of the border) shows the formation of elongated, larger RDX crystals. The onset of crystallization of the deposited RDX sample was observed immediately, even after a single TIJ pass. RDX crystal formation was observed only at the edges (inner and outer rim) of the deposited sample on the substrate. Although crystallization was observed to a small degree and only at the substrate edges, the solvent mixture used was considered adequate for the depositions and was left unchanged. The idea of decreasing the dispensing solution concentration and increasing the numbers of passes to increase the surface loading concentration also led to crystallization, as was demonstrated by Manrique-Bastidas and collaborators for TNT (Manrique-Bastidas et al. 2004a; Manrique-Bastidas et al., 2004b). However, this behavior is not general, and each case depends on the solvent mixture/HEM combination. For example, the high affinity of AN for water made its deposition onto surfaces a challenge.

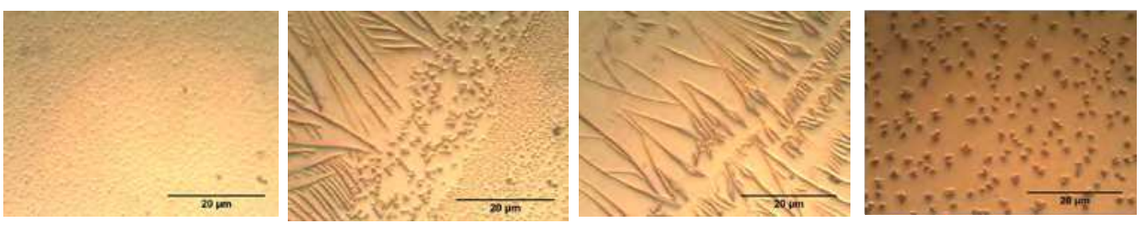

a. Center: 1 pass b. Inner Edge c. Outer Edge d. Center: 5 passes

Fig. 5. White light microscope images of TIJ-deposited RDX on a gold-silicon substrate: (a) center section of the substrate; (b) inner edge of the substrate; (c) outer edge of the substrate. (d) center section of the substrate after five TIJ pass. The conditions included a stock solution of 892 ppm RDX and a solvent consisting of 10% ACN, 20% MeOH and 70% IPA. The image was acquired at an optical magnification of 100×.

Although water is the optimum solvent for TIJ because of its high surface tension and low viscosity, attempts to dispense aqueous solutions of AN resulted in poor spreading of the deposited analyte/solvent mix over the surface; instead of spreading evenly, the mixture remained in isolated droplets on the surface. Fig. 6 depicts the micrographs of the results of dispensing AN on gold-silicon substrate using a solvent mixture of 10% H_2O and 90% IPA. The results were similar after one TIJ pass (Fig. 6a) and five TIJ passes (Fig. 6b). The lack of homogeneity of the distributions obtained can be clearly observed. Instead forming of a uniform layer of analyte on the surface, the formation of dispersed, isolated droplets is favored. When initially deposited, the droplets were much more finely dispersed, but

moisture in the air was enough to induce the formation of larger droplets on the substrates. Because of the problems related with using water as the solvent for depositions of AN, a solvent mixture was prepared containing 12% MeOH and 88% IPA. The appearance of AN in this solvent mixture after dispensing onto the gold-coated silicon slides is depicted in Fig. 6. The difference in comparison to the water-based solvent mix can be clearly seen as a collection of fine and uniformly dispersed deposits, especially along the edges. While absorption of water from the atmosphere was still taking place in the center of the substrate, this process occurred to a much smaller degree than in the samples deposited with AN/water solutions only. The conditions included a stock solution of ~ 812 ppm AN and a solvent consisting of ~ 10% H_2O and 90% IPA. Optical magnificationused was 10×. White light 100× magnification micrographs of TIJ deposits of 1059 ppm TNT in MeOH after 25 passes: (c) edges; (d) center.

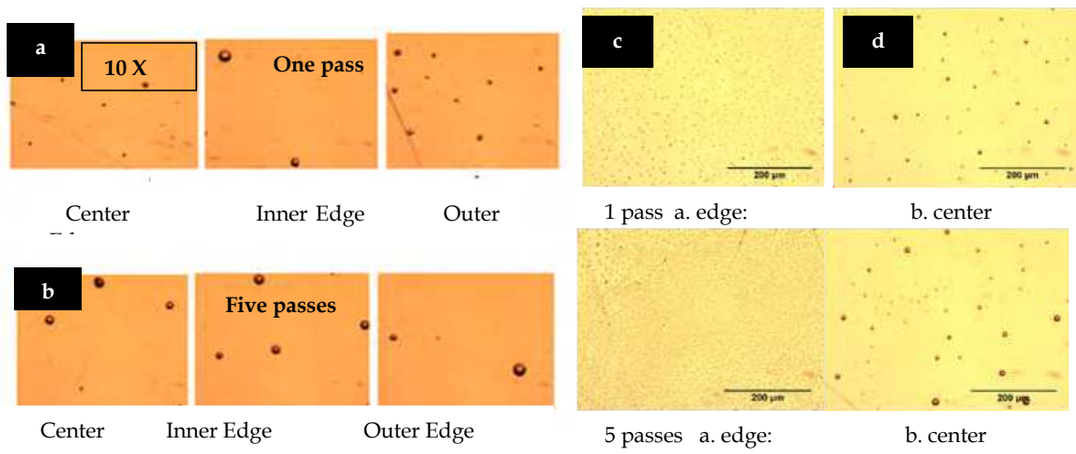

Fig. 6. White light micrographs of TIJ deposits of AN onto a gold-silicon substrate. (a) one TIJ pass; (b) five TIJ passes. The conditions included a stock solution of ~ 812 ppm AN and a solvent consisting of ~ 10% H2O and 90% IPA. The optical magnification is ~ 10×. (c) one TIJ pass; (d) five TIJ passes. The conditions included a stock solution of ~ 812 ppm AN and a solvent containing ~ 12% MeOH and 88% IPA. The optical magnification is ~ 10×.

Smearing deposition has been used as a method for sample preparation of solid compounds on substrates. Samples and standards of nitrocompounds [7, 9] and cyclic organic peroxides as well as pharmaceutically active ingredients and excipients have been prepared (Primera-Pedrozo et al., 2004). These studies centered on covering relatively large surface areas (~43 cm^2) on stainless steel, aluminum or glass (Hamilton et al, 2005; Perston et al., 2007). In all mentioned applications, smearing proved to be a high-quality deposition technique as judged by the excellent agreement between the amount aimed to be deposited, the actual amount deposited, coverage uniformity and the percent of analyte recovered after substrate rinsing. The introduction of TIJ to design new methodologies for preparation of samples and standards required a comparison with the well established sample smearing technique. As already mentioned, samples were prepared by both deposition methods using the same solvent mixtures to make a real comparison. After sample preparation, the substrates were rinsed and analyzed using

protocols based on HPLC or IC in order to determine the total mass collected in the solution. Results obtained from the chemical analyses were then expressed in terms of surface loadings (μg/cm^2).

The images acquired after each carrying out each method were excellent tools in assessing the performance of the methods. In general, smearing was a somewhat inconsistent process because it relies on human intervention to be carried out. At times, even the environment in which the method took place altered the reproducibility. Examples including wind drifts from a fan or high lab humidity altered the way in which the solution adhered, spread out or dried on the substrate surface. The smearing process was more exposed to the local environment than the TIJ method because surface depositions using the latter technique took place within a custom acrylic built covering with a controlled atmosphere. Images were acquired at several locations. Another important observation during smearing depositions on these substrates was the poor adhesion of the HEM studied to the gold coated silicon surface, in contrast to the strong adhesion experienced by analytes (including nitrocompounds and cyclic peroxide HEMs) to other test surfaces such glasses, stainless steel, aluminum and plastics. Solid-phase residues of HEM were often left on the Teflon applicator after smearing was performed in one or two passes. This residue was considered an indication that the surface used in the experiments was very inert and thus rejected the adhesion of the analytes.

Images acquired of thermal inkjet depositions showed entirely different results compared to smearing. TIJ reduced significantly the direct operator interaction during the deposition process. Thus, reproducible results with uniform surface concentrations were obtained for TIJ depositions. Figure 5 shows an even distribution of TNT/10% ACN, 20% MeOH and 70% IPA droplets on the right edge and center of the substrate after dispensing. It is possible to observe slight differences in various areas depending on the location of the deposited sample on the substrate, but overall, even surface concentration dominated the depositions. An interesting finding was that the droplets were in a metastable state (similar to super cooled water in a refrigerator) instead of in the assumed crystalline state (Manrique-Bastidas et al. 2004a; Manrique-Bastidas et al., 2004b). As a result, the images captured show the TIJ method of deposition to yield more favorable results than smearing with respect to achieving consistent homogeneous surface concentrations.

Both deposition methods have positive and negative aspects. Smearing is fast and easy to use. Typically, it has a relatively high susceptibility to human error, at times leading to irreproducible results, and requires large amounts of time for dispensing a wide range of concentrations. Moreover, it produces poor surface loading concentrations over surface areas of ~ 1.0 cm^2 and smaller on highly inert surfaces such as gold coated silicon. As can be observed in Table 2, only between 29% and 70% of the deposited material could be recovered after deposition by rinsing and subsequent HPLC analysis. The highest deposited surface concentration tested in this work (50 μg/cm^2) was very difficult to achieve because of the low adhesion of TNT to the small sample area of the surface and the high affinity of TNT for the Teflon applicator. These characteristics explain why the lowest percent recovery (37% – 55%) was obtained for this surface loading. Deposition of extremely low concentrations of approximately 1.0 μg/cm^2 failed because the small volume of HEM in solution was not enough to cover the entire surface, without modifying the protocol established. This could be attributed to the fact that the pressure applied to the substrates or the speed of spreading are both operator-dependent. Also, because the deposition takes

place in the open air, explosives with high vapor pressures would sublimate quickly during this procedure. Thus, smearing was prone to a large degree of human variability during its preparation stage.

Deposited (μg/cm²)	Recovered (μg/cm²)	Recovered (%)
50	29.8 - 18.8	37.6 - 55.7
10	6.1 - 7.1	60.6-70.9
5.0	2.9 - 3.6	57.8 - 71.4
1.0	0.3 – 0.7	29.8 - 66.3

Table 2. Comparison of the theoretical amount of TNT deposited using smearing and the real surface concentration detected after rinsing.

TIJ, however, has a small margin for operator error, resulting in reproducible and even surface loadings. TIJ also has the possibility of becoming even more useful in conjunction with simple programming. Different shapes, different surface loadings on the same substrate and the spacing between deposited areas can all be optimized using this technique, whereas sample smearing has fewer degrees of freedom available for improvement. Thus, with respect to overall ease of use and functionality, TIJ was demonstrated to be the superior method of deposition when compared to sample smearing. Sample deposition using TIJ was time consuming for high surface loadings, even for a substrate of only 0.8 cm². Each successive pass required the operator to manually push a button that alerted the software to perform another pass. Thus, although depositions with TIJ can take a significant amount of time, particularly for high surface concentrations, the operation results in high mass transfer yields and there is a finer control over the place where the dispensing takes place. The TIJ dispenser took roughly 14 s to complete a single pass on the 0.8 cm² surface area, and, depending on the behavior of the solutions used, some depositions required a delay of up to 60 s between passes to allow the sample to dry.

The main advantage offered by TIJ is that, in principle and in practice, only one concentration is required for dispensing a broad range of surface loadings, reducing significantly the errors associated with operator intervention and with the preparation and use of multiple dilutions. In this work, it was estimated that HEMs stock solutions of concentrations in the range of 800 to 1100 ppm would result in loadings of the desired surface concentrations so that each TIJ pass added an easily traceable amount. The devised protocol proved to be very simple and limited the number of steps in the methodology. In addition, the number of TIJ passes controlled the surface loading concentration very efficiently, as shown in Table 3 for TNT. For example, after performing one TIJ pass using a 1059 ppm TNT stock solution, 1.04 μg/cm² were deposited onto the gold-silicon surface. In Figure 6, the relationship between the number of TIJ passes and the surface loadings for the HEMs studied is represented. The deposition of RDX and TNT exhibited linear behavior with respect of the number of TIJ passes applied to the substrates, but the deposition of AN stock solutions with TIJ was not.

This non-linear behavior of AN was attributed to the affinity of the analyte for water in the form of ambient humidity; as time passed, AN absorbed additional water from the air. This phenomenon would explain why, when more AN was available, the surface concentration began to increase exponentially, but the precise reason behind this behavior is currently unknown. These results demonstrate that, using the TIJ method, it is possible to generate samples and standards of HEMs with more uniform coverage and surface loading concentrations that can be varied by changing the numbers of TIJ passes without the need for serial dilutions. Attempts to prepare standards lower than 5 μg/cm² for AN were unsuccessful because that solution, after rinsing, was outside of the lower value of the IC calibration range (1.0 ppm). As explained above, for TNT there was a direct relationship in the number of passes and loading concentration. For TNT, one pass resulted in a surface loading of 1.0 μg/cm², and 10 passes led to a surface concentration of 9.2 μg/cm². For RDX, one pass led to 0.55 μg/cm², five passes generated a loading of 3.2 μg/cm² and 10 passes resulted in a deposition of 5.4 μg/cm². This result confirms that the amount dispensed by TIJ is markedly dependent on the substance to be deposited and also on the solvents and surfaces used for the depositions.

Number of passes	Rinsing Vol. (mL)	Loading concentration (μg/cm²)
1	5	1.04
2	10	2.08
5	10	5.58
7	10	7.88
10	10	9.19

Table 3. HPLC analysis of TNT loading concentrations obtained by varying the number of TIJ passes.

Even though TIJ promises to be a good method for the preparation of samples and standards on surfaces, maintenance of the TIJ print is a potential problem, and care must also be exercised when re-using solutions stored in the cartridges. If the cartridges are not properly sealed after use, then the solutions could leak out of the nozzles and solidify, clogging the pores of the inkjet cartridge. This clog eventually could lead to disruptions in the depositions of the desired surface concentrations upon further use.

The shelf life is a critical parameter to evaluate during the production of samples and standards of solid analytes deposited onto substrates. Materials with high vapor pressure will not stay on the surface for a long time. However, the sublimation of the material depends on the material-surface interactions. TNT, which has a higher vapor pressure than RDX, will sublimate faster than RDX. As will be shown, RDX stays on the stainless steel surface for almost an entire year without any significant changes of the FTIR band intensities (expressed as peak areas). Another significant parameter to be considered is the photodecomposition of analytes by exposure to light (Irrazabal et al., 2007) leading to the formation of new products. To perform comparisons of surface effects, samples were dispensed using TIJ onto gold coated silicon, glass and stainless steel (SS) substrates. Three samples of TNT were prepared on each

surface using 10 passes, leading to a final surface concentration of approximately 10 μg/cm². The samples were then analyzed by OFC-GAP/FT-RAIRS for 900 min (15 hr) to examine sublimation from the test surfaces. In the case of RDX, experiments were performed over 11 months after smearing on a SS substrate. Figure 7 shows the RAIRS spectra of 10 μg/cm² TNT on glass, SS and gold-silicon surfaces. The vibrational signatures of the HEM can be clearly observed (1096 cm^{-1}, 1181 cm^{-1}, 1354 cm^{-1}, 1559 cm^{-1}) (Lin-Vien et al., 1991). The nitro symmetric stretching vibration of TNT band appeared at 1354 cm^{-1}, and the nitro asymmetric stretching vibration was found at 1559 cm^{-1}. The locations of persistent IR bands were almost the same on the different test surfaces, with only a few changes in intensity. The presence of a strong band at about 1267 cm^{-1} can be attributed to Si-O vibration in the glass. The spectra of TNT on gold-silicon are shown at 0 hr and at 15 hr, after completing the sublimation studies. At 15 hr, the TNT vibrational signatures disappeared from the spectrum, indicating that the compound had sublimated from the surface.

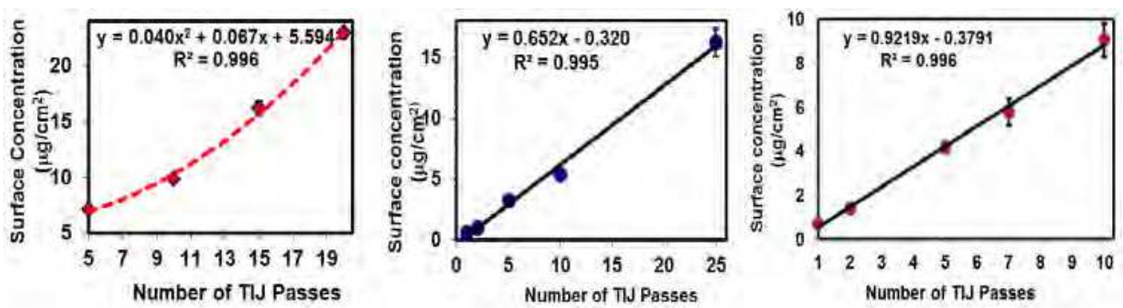

(a) (b) (c)

Fig. 6. Surface loadings obtained by variation of the number of TIJ passes dispensed to gold-coated silicon substrates. (a) AN, 892 ppm; (b) RDX, 812 ppm; (c) TNT, 1059 ppm.

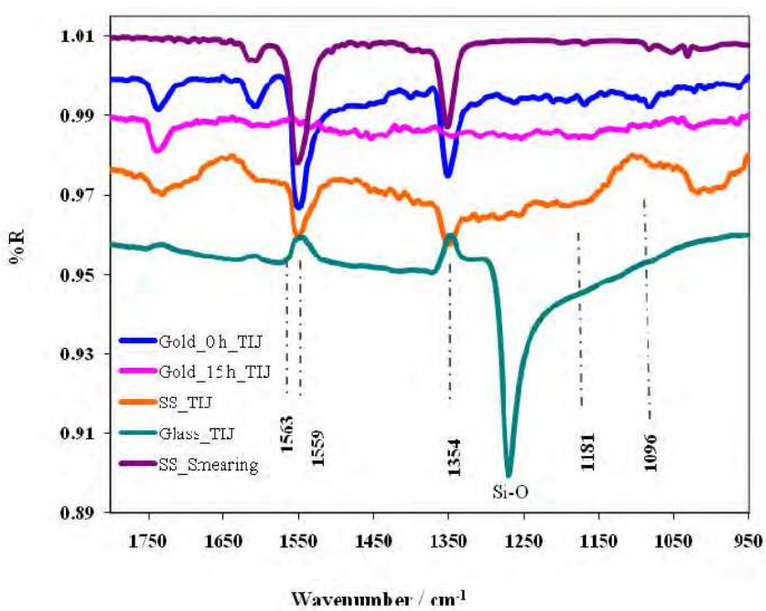

Fig. 7. FTIR spectra using a grazing angle objective for 10 μg/cm² RDX (smearing) and TNT (TIJ): (a). RDX/SS; (b) TNT/Au@Si, 0 h; (c). TNT/Au@Si, 15 h; (d) TNT/SS; TNT/glass.

Sublimation rate studies were performed for TNT deposited onto the mentioned surfaces. Peak areas were calculated for the IR band centered at 1354 cm^{-1} using the OPUS™ Bruker Optics software (Billerica, MA) for all the spectra recorded over 15 hr. Peak areas were calculated by integration using straight lines that connected the wavenumber limits of the peak envelopes as baselines. These results are shown in Figure 8 for TNT on SS, glass and gold-silicon. In the same graph, the sublimation behavior of RDX (in days) is observed (the *x* axis is on the top of Figure 8).

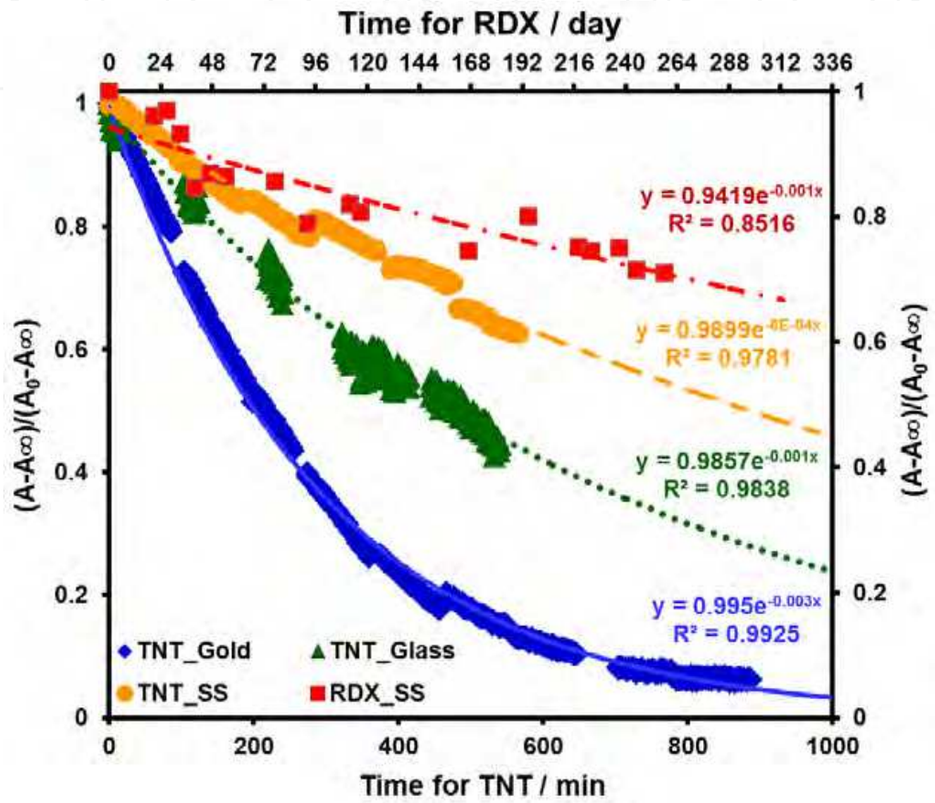

Fig. 8. Plots of $(A-A_\infty)/(A_0-A_\infty)$ vs. time for surface sublimation for: TNT on gold-silicon (♦); TNT on glass (▲), TNT on stainless steel (●) and RDX on stainless steel (■).

According to standard procedures in kinetics and dynamics measurements, a physical property can be taken to be directly proportional to the concentration of a given species in the concentration range used. In the present studies, integrated IR band areas were taken to be directly proportional to the surface concentrations. In Equation 1, A_∞ is the area at infinite time, A_t is the peak area at time t (given in seconds) and k is the surface sublimation constant. The decay of peak areas was monitored as a function of time for the different surfaces, and the data were plotted as ln (A_t-A_∞) vs. t. The surface sublimation constant was obtained from the value of the slope for the linear regression trend.

$$ln\,(A_t - A_x) = kt \tag{1}$$

The data were adjusted to Equation 1, and the value of the constant parameter k was calculated. The results are shown in Table 4. The residence time of the explosive on the

surfaces (gold on-silicon, glass and SS) is affected by the sublimation process, vapor pressure (Phares et al., 2000) and HEM interaction with the surface. The residence time (RT) can be described as the time the material will persist on a surface after exposure to ambient conditions. The results indicate that TNT on SS has a residence time longer than the other surfaces studied. The half life values (t_{50}) for surface residence are also shown in Table 4 for TNT on gold-silicon, glass and SS surfaces and for RDX on SS. Residence time half life values for TNT on glass and SS are higher than on gold-silicon. These results are closely dependent of the material type. Gold on silicon is a very inert surface compared to glass and SS surfaces. This caused the poor adhesion of the material on the gold-silicon indicating that the interaction between the HEM and substrate is stronger in glass and SS than gold on silicon. However, for the gold coated silicon surface, this interaction should be minimal, due to small value of t_{50} = 195 min. The high value of 630.1 days for t_{50} of RDX is an indication of strong interactions between the HEM and the stainless steel surface compared to gold on silicon, and it is closely related to the low vapor pressure of RDX.

Kinetics Parameters	TNT @ Gold (min)	TNT @ Glass (min)	TNT @ SS (min)	RDX @ SS (day)
k	0.00356	0.00142	0.00081	0.0011
$t_{1/2}$	195	488	857	630

Table 4. Kinetics parameters of the sublimation of TNT on different surfaces and RDX on SS.

The results presented above confirm that physical properties such vapor pressures and surface type influence the lifetime of the highly energetic materials on the substrates and the practical limits of substrates for preparation of samples and standards. Although AN was not tested in sublimation studies, it is estimated that it will remain on the surfaces for a long time due to its ionic character and low vapor pressure. However, the high affinity for water constitutes a practical limitation, particularly if the samples/standards are meant to be used for IR detection applications.

3. Detection of hazardous liquids concealed in commercial products by OFC-Raman spectroscopy

In August 2006 a terrorist plot to destroy aircrafts on transatlantic flights was discovered and timely stopped in London. The plan involved the use of liquid explosives stored in beverage bottles that would pass check points without being detected. The liquids were going to be mixed in flight, generating an improvised explosive device (IED) and were going to be left in the aircraft and detonated remotely after the aircraft landed (CNN news report, 2006). Immediately, airport security agencies at UK and USA established a ban to all liquids except from medicine and infants food beyond checkpoint. The position has been changed several times to allow certain amount of liquid or gel based products. However, when or how terrorists would try to pass hazardous liquids into an aircraft to create a threat, explosive or chemical is uncertain. For this reason it is important to develop a methodology through which it would be possible to differentiate between common products and compounds that can be combined for terrorisms intends.

The use of hazardous liquids as tools for terrorist intentions is not a new modality. Terrorists have used hazardous chemicals that are liquids at room temperature in many

occasions. Some examples are the bombing to the World Trade Center in 1993, the attempt to a Philippine Air flight in 1994 and the deployment of the CWA Sarin in a Japan subway in 1995. Some of these attempts involved the use of liquid explosives like nitroglycerin and other nitro compounds. Peroxide based explosives are also easily prepared from common liquids such as acetone. Other extremely hazardous liquids are chemical warfare agents (CWA) and Toxic Industrial Compounds (TIC). TICs are chemicals toxic to humans that are widely used in manufacturing or primary material processing. They have received more attention in recent years because ease of accessible in large quantities by potential terrorists. Chemical warfare agents (CWA) differ from TICs in that they are intended to immediately incapacitate as many soldiers as possible when released against an enemy in war. To do this, the CWA must be toxic enough to cause an instant response when it is inhaled or comes into contact with the skin. Table 1 contains examples of some hazardous liquids and their volatility. Highly volatile materials can be easily deployed just by opening the container. Along with the volatility of these chemical is the Immediately Dangerous to Life or Health (IDLH) level and is defined by the US National Institute for Occupational Safety and Health. This value is the concentration in air that would cause immediate or delayed adverse health effects after 30 min of unprotected exposure. If these chemical are used in large quantities toward civilians, the amount of casualties will be huge. However even small quantities of a toxic chemical or a small IED can cause chaos specially in closed environments like an aircraft or a train or high transit areas like a building or a transportation terminal.

Chemical	Description	Volatility (mg/m^3)	IDLH (ppm)
GB ($C_4H_{10}FO_2P$)	CWA: Sarin, organophosphate nerve agent.	16,091	.03
AC (HCN)	CWA: hydrogen cyanide, blood agent	1,080,000	50
HNO_3	TIC: nitric acid, a highly corrosive acid	63,000	25
H_2SO_4	TIC: sulfuric acid, a strong mineral acid	1.3	3.7
GD ($C_7H_{16}FO_2P$)	CWA: Soman, a nerve agent	3,900	.008
PCl_3	phosphorus trichloride	130,000	25

Table 5. Description of liquid CWA and TIC at room temperature.

Various approaches have been taken to detect and identify chemical agents including HPLC/MS GC/MS, Ion Mobility Spectroscopy, Infrared Spectroscopy and Raman Spectroscopy (D'Agostino et al., 2006; Sun and Ong, 2005, Marrs et al., 1996). Vibrational spectroscopy has the advantage that provides chemical information and provide with the sensitivity and selectivity required for Chemical Point Detection systems and has the potential for remote sensing. Specifically, Raman is able to analyze samples though various transparent glass and plastic containers, such as beverage bottles or food containers. This allows the contents of a container to be analyzed without opening the container, minimizing exposure to potentially harmful substances and helping to speed the screening process. In this work concealed liquids scenarios are studied by Raman spectroscopy. Hazardous liquids including CWAs TICs and other prohibited are studied through the walls of commercial drink containers. Fiber optic coupled Raman was used to evaluate the content of plastic and glass containers. Standoff Raman detection was used to obtain information of

hazardous liquids and mixtures from 20 feet distance. The objective of this work is to study, in real field conditions, the detection of CWAs and TICs by point detection or with a as a remote surveillance tool.

Raman spectroscopy is one of the promising tools under consideration (Fraquharson et al., 2005; Pearman and Fountain, 1999). Since Raman scattering brings information on vibrational modes of molecules it can be used as a specific mean of detection. These days, Raman systems are portable, sensitive, flexible tools that are used in the field and the laboratory (Marrs et al., 1996). Raman based systems are able to analyze samples through various transparent glass and plastic containers (US NRC, 2004). This allows the non-invasive, non-destructive inspection of the content of a container without opening, minimizing exposure to potentially harmful substances and helping to speed the screening process. Also water does not present a strong signature in Raman measurements therefore Raman based systems result attractive to characterize aqueous based commercial products.

In this study Optical Fiber Coupled Raman spectroscopy (OFCRS) was used to characterize samples where a hazardous liquid is concealed either in a commercial product container or mixed with consumer products. Several commercial consumer products such as: mouthwash, sodas, juices and liquors were mixed with liquid explosives, flammables and CWA's. FOCRS was used to evaluate the content in plastic and glass containers. The dependence on liquid color, container material was also studied. The results suggested that the technique can be used to discriminate if the commercial liquids are the intended or a hidden hazardous liquid.

Raman spectroscopy presents various strengths that make it a potential technique for detection of chemical agents in the field. Since Raman scattering brings information on vibrational modes of molecules it can be used as a specific mean of detection. Water does not present a strong spectra making possible to analyze a variety of samples where water can be interference. In 1999 Christensen reported the use of a portable Raman system to characterize chemical agents sealed on glass containers. Samples were part of a library for military training in chemical agent identification. (Christesen et al. 1999). Optic fiber coupled Raman spectroscopy (OFCRS) was used to characterize liquid explosives and commercial liquids (Alvarez-Rivera, 2002). The results suggested that the technique can be used to discriminate if the commercial liquids are the intended or a hazardous liquid. Eliasson and colleagues (Elliasson et al., 2007) have reported the detection of drugs and liquid explosives concealed in dense colored plastic containers. The technique consists of a variation of the angle of detection to collect scattered Raman radiation. This approach allowed reducing fluorescence and interferences.

In 2002 Harvey evaluated a portable Raman system for forensic applications (Harvey et al, 2002). The evaluation of chemical agents in glass and plastic vials included library matches and variability due to containers and the use by operators. The third component of the present work is to evaluate Raman as a detection tool for concealed hazardous liquids. Liquid explosives and chemical agents were detected in a variety of consumer product containers either pure or missed with the commercial product.

The hazardous materials used for the detection experiments were: hydrogen peroxide 50% wt. in water, toluene, benzene and 99.5% ethanol from Aldrich chemicals. Also, acetone, dimethylmethyl phosphonate (DMMP) and triethyl phosphate (TEP) from Fisher Scientific were used. Fisher chemicals were obtained from Fisher Scientific International, Chicago, IL. Aldrich chemicals were obtained from Sigma-Aldrich Chemical Company (St. Louis, MO).

DMMP and TEP are structural analogs of chemical warfare agents (CWA) such as TABUN, SARIN, SOMAN, and GF and therefore are commonly used as CWA simulants (CWAs). The commercial liquid products employed in this study were: Gatorade variety drinks (distributed by The Gatorade company, Chicago, USA), Scope mouthwash (distributed by Procter and Gamble, Cincinnati, USA), Dewar's White Label whiskey (imported by Mendez & Co., PR), Ron Bacardi light rum (Produced by Bacardi Corp, PR), V8 vegetable juice (distributed by Campbell Company, NJ, USA), 7Up (distributed by Coca Cola Company, Puerto Rico). The effect of thickness and color of commercial glass and plastic containers were evaluated (See Table 2 for details). Raman spectrum of the original liquid in its container was obtained. Then the liquid was replaced by a hazardous liquid or mixture. Light absorption of containers at different wavelengths was studied.

Container	Material	Description
green glass bottle	glass	soda water (Canada Dry®)
amber glass bottle	glass	Malt beverage (Malta India®)
clear glass bottle	glass	Perfume (Adidas®)
clear glass bottle	glass	Juice (Snapple®)
blue plastic bottle	Plastic (PET)	Water (Aquacal®)
green plastic bottle	Plastic (PET)	Refreshment (7up®)
clear plastic bottle	Plastic (PET)	Baby bottle
clear plastic bottle	Plastic (PET)	Perfume (Ralph® body spray)

Table 6. Description of containers used in the OFC-Raman spectroscopy experiments.

A Renishaw RM1000 system microscope with a NIR 785 nm laser was used to obtain the spectra of explosives mixtures. The Raman shift spectra were obtained from 200 to 3200 cm^{-1}. The system was calibrated using silicon single crystal sample as an external standard by measuring the vibration at 520.56 cm^{-1}. Two portable fiber optic Raman spectrometers (Raman Systems R-3000 HR) were used to evaluate the spectral signature of commercial products. The excitation wavelengths used were 532 nm (green) with 25 mw maximum output power and 785 nm (red) with 250 mw maximum output power. The spectra of the original liquid in its container was collected though the walls. A volume of 30 mL of a hazardous liquid compound was then transferred and analyzed in different commercials containers varying the time and the power. Raman spectra were acquired from 200 cm^{-1} to 1800 cm^{-1}. The systems were calibrated using cyclohexane.

The spectra of three liquors were obtained in the same clear glass bottle. The results are presented in Fig. 9a. As expected the rum, gold tequila and whiskey present the same spectra. The yellowish color of the tequila and whiskey presented some fluorescence identified by the shift in the baseline of the spectrum. However it is possible to identify the main peaks associated to the alcohol content. These spectra as well as the spectrum for ethanol, the main component of hard liquors, present peaks at 881(C-C-O stretch), 1048 cm^{-1} (ring vibration), 1186 and 1280 cm^{-1} (ring stretch) and 1456 cm^{-1} (CH_3 deformation). Then the content of the clear glass bottle was replaced with acetone and hydrogen peroxide so that the content appears to be clear rum. These products can be easily found at beauty supplies and drugstores. These are commonly found in consumer products such as nail polish remover and hair care products. However together they can be mixed to for acetone peroxide, a known homemade explosive. The Raman spectra of acetone, peroxide and the

acetone peroxide explosive are presented in Fig. 9b. Acetone's main peak is located at 789 cm^{-1}. For peroxide the strong Raman line at 878 cm^{-1}, characteristic O–O stretching mode, is stronger than that the other peaks of the spectra. For the AP the main peaks are located at 588 cm^{-1}, and three characteristic peaks at 780 cm^{-1}, 890 cm^{-1} and 936 cm^{-1}. The position and intensity of the major peaks in acetone and peroxide make them easily detected by Raman and can be used as markers for explosive mixtures.

Fig. 9c presents the Raman spectra of 20% and 60% peroxide in whiskey. As previously mentioned, the spectroscopic signature of peroxide is hidden or masked by the whiskey. Samples from 0% to 90% peroxide in whiskey were prepared without changing the location of peaks. Since the presence of peroxide increased the intensity at 874 cm^{-1} the peaks ratio can be used to discriminate between the original liquid and adulterated liquor. OPUS PLS Package was used to build a model to determine the concentration of peroxide in whiskey. The result of the cross validation is included in Figure 10a. The data from these same samples was correlated just for presence of peroxide. The graph at Figure 10b confirms that peak ratios can be used to discriminate between an original liquid and a concealed hazardous material.

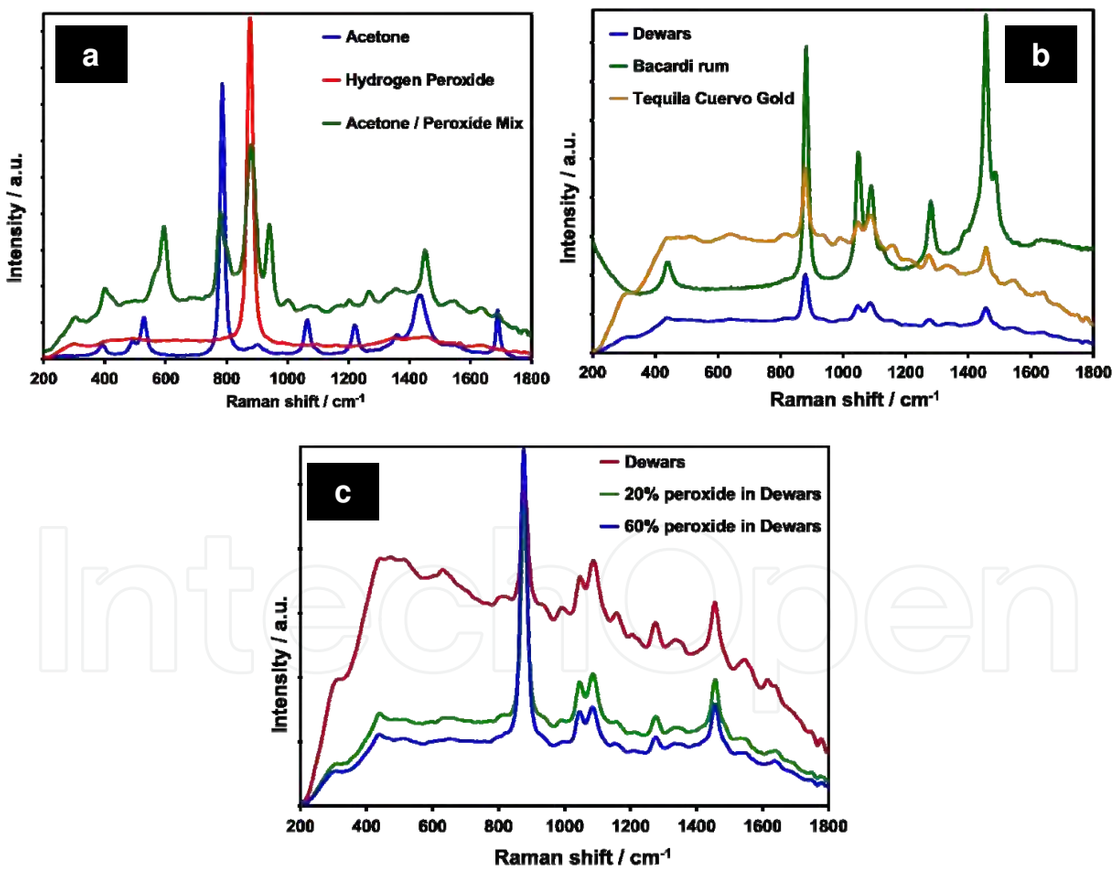

Fig. 9. (a) Raman spectra of liquors in their original containers acquired with optical fiber probe. (b) Raman spectra of acetone, peroxide and acetone peroxide explosive in a clear glass bottle; (c) Raman spectra of a mixture of hydrogen peroxide and Dewar's whiskey. Conditions: 785 nm laser, 200 mW power and 2 s integration time.

The spectra of a perfume and Plax™ mouthwash are shown in Fig. 11. Intensity of the peaks is reduced by the fluorescence of the liquid. Most noticeable peaks for the mouthwash appear at 875 cm^{-1}, 1000 cm^{-1}, 1080 cm^{-1}, and 1450 cm^{-1}. For the perfume the sharper peaks are: 798 cm^{-1}, 878 cm^{-1}, 1260 cm^{-1}, 1090 cm^{-1}, 1450 cm^{-1} and 1610 cm^{-1}. Consumer products such as personal care and cosmetics present a challenge. Commonly these products contain ingredients such as alcohols, peroxides and others with chemical composition related to hazardous chemicals. Also these liquids are usually colored and present fluorescence.
The perfume bottle was emptied and replaced by several toxic industrial compounds. Fig. 11b shows the detection of toxic industrial compounds using a 532 nm laser. These liquids will exhibit strong peaks that will differentiate the material from the original liquid (perfume). The spectra of dimethyl methyl phosphonate (DMMP), a chemical warfare agent simulant is shown in Fig. 12a. This spectrum was collected through the walls of a clear glass juice bottle (Snapple) and was detected using 532 nm laser beam with 10 mW and the acquisition time was 1 s for recording the spectrum. The peaks at about 715 cm^{-1} for DMMP correspond to a stretching mode involving the phosphorus atom. Fig. 12b shows the OFC Raman spectrum of the chemical agent simulant triethylphosphate (TEP).

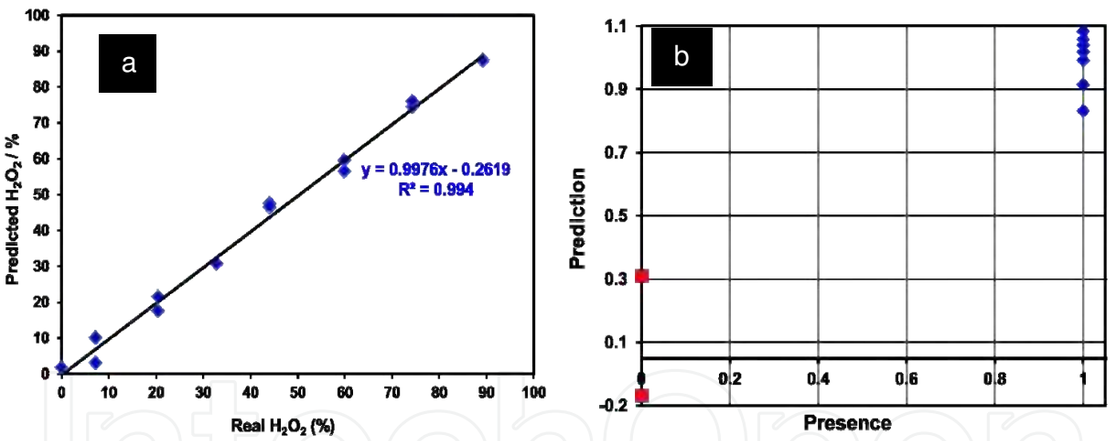

Fig. 10. (a) Prediction of the concentration of peroxide in whiskey; (b) prediction of presence of peroxide in whiskey.

The Raman spectrum of acetone was collected in different bottles using the same acquisition parameters at 532 nm (Fig. 11a) and 785 nm (Figure 11b) laser source. The characteristic peaks of acetone at 780 cm^{-1}, 1400 cm^{-1} and 1700 cm^{-1} were observable for all samples. However for 532 nm data the intensity of the peaks decreased in the following order: clear glass > clear plastic > green glass > amber glass. When the 785 nm laser was used the order was: clear glass > clear plastic > amber glass > green glass. It was not possible to collect a spectrum of the chemical in the green glass bottle using 30s of 200 mw of 785 nm laser power.

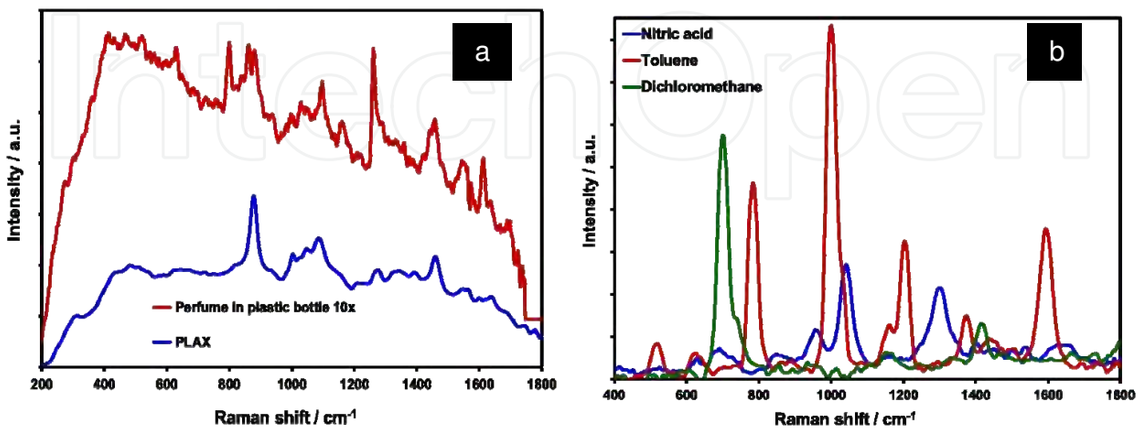

Fig. 11. (a) Raman spectrum of a perfume and mouthwash acquired with optical fiber probe; conditions: 785 nm laser, 100 mW and 1 s of integration time. (b) Raman spectra of toxic compounds within a perfume clear glass bottle at 532 nm, 1 s and a laser power of 12 mW.

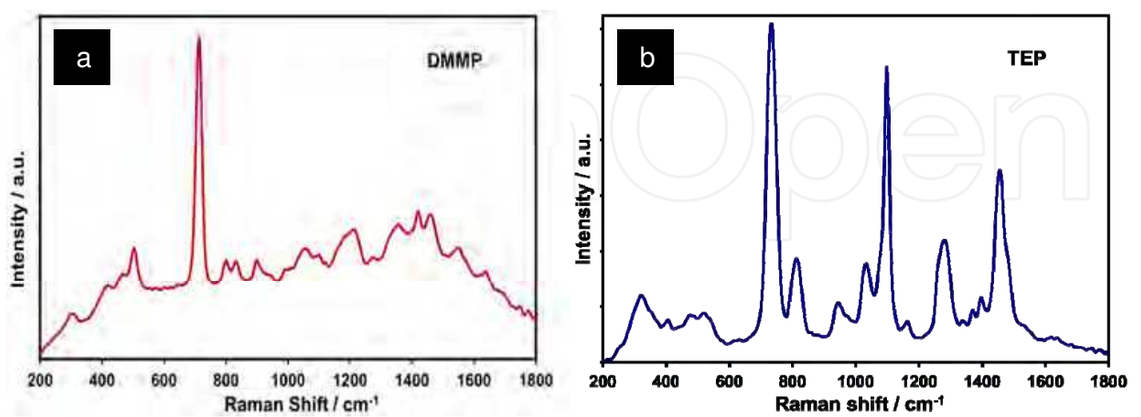

Fig. 12. Raman based detection of chemical agents simulants in a clear glass bottle at 532 nm laser, 1 acquisition, 1 s, 10 mW: (a) DMMP; (b) TEP.

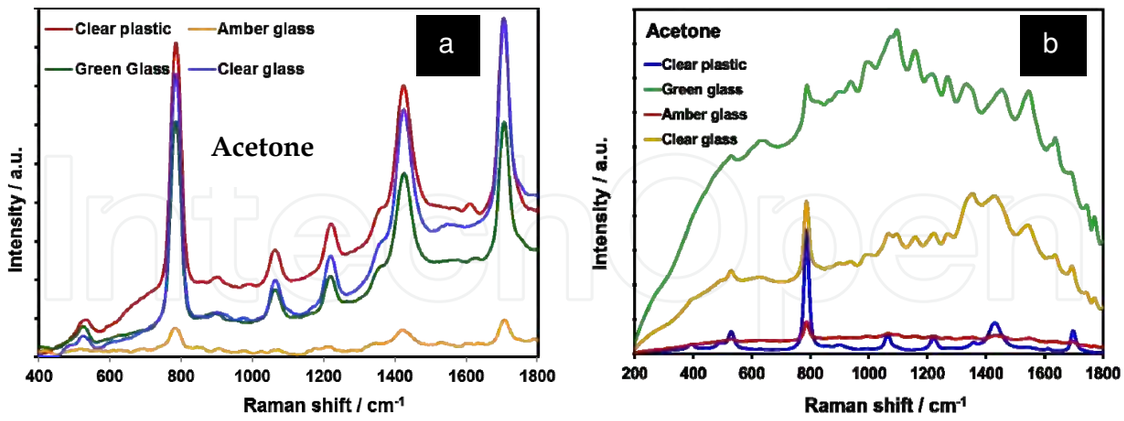

Fig. 13. Raman spectra of acetone in different bottles. (a) 532 nm 20 s, 33 mW; (b) 785 nm 30 s at 200 mW.

Since it was possible to collect a spectrum from the green plastic bottle, the behavior could be associated to thickness of the walls. The thickness of glass and plastic bottles was measured. Table 7 present the results that are similar among glass bottles and differing considerably from a water plastic bottle.

Product	Material	Color	Thickness (mm)
water	plastic (PET)	clear	0.22 ± 0.02
fruit juice	glass	clear	1.92 ± 0.42
malt beverage	glass	amber	2.28 ± 0.44
beer	glass	green	2.02 ± 0.47

Table 7. Thickness of common containers evaluated with OFC Raman.

Then the region between 700 cm^{-1} and 900 cm^{-1} of acetone was used to study the effect of different collection parameters on the spectra inside different bottles. The acquisition time was changed from 1 to 30 s. The laser power was varied from 11 to 32 mW. The power intensity of the instrument modulating and the output power was measured at the probe with a digital power meter. At fixed laser power of 18 mW the response was linear with increasing acquisition time (Figure 14). For the amber glass bottle the increase in peak area was significantly lower. This suggests that the bottle color is responsible for the fluorescence.

The transmission spectra of different bottles are shown in Fig. 15. These spectra were acquired in the 220 nm to 1200 nm range. The objective of this experiment was to measure how much light is allowed transmitted in a specific bottle at different wavelengths. Solid vertical lines represent the laser wavelengths evaluated in the present work and dashed vertical lines mark the wavelength range for Raman spectra with shifts from 200 to

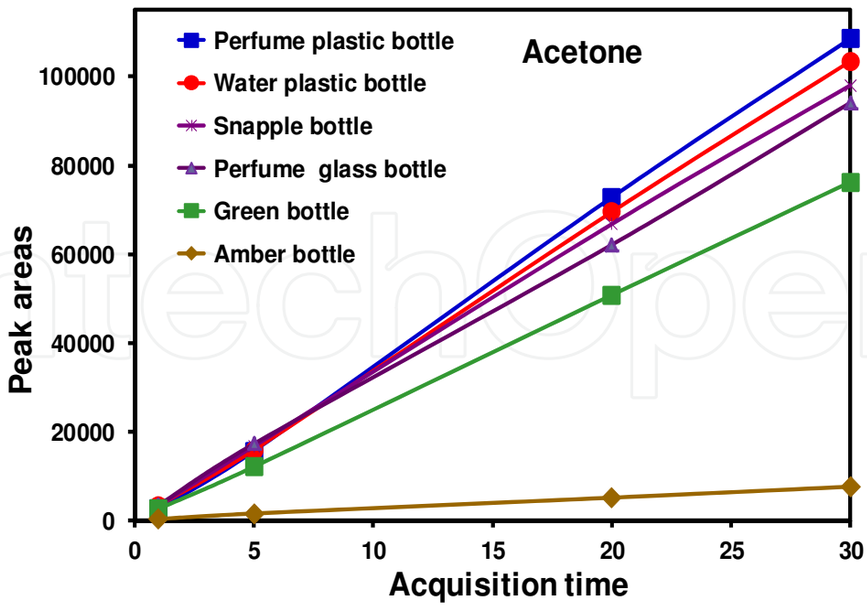

Fig. 14. Detection of acetone at different collection times inside different bottles at 532 nm and 18 mW (1 scan).

1800 cm^{-1}. According to this illustration all clear containers (glass and plastic) will allow light of all wavelengths to reach the container as well as allow detecting scattered radiation. However for amber containers the optimum range for interrogation will be 600 to 750 nm. The comparison with green containers suggests that the container material absorbs most of the light but a spectrum of the content would be possible with the appropriate laser power.

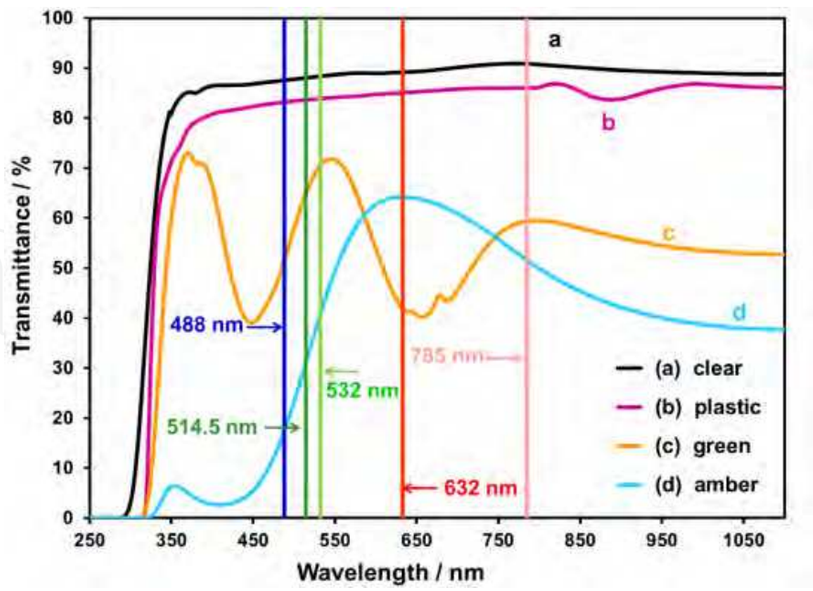

Fig. 15. Transmission spectra of different bottles materials. Solid vertical lines indicate excitation lines in Raman experiments. Dashed lines indicate range for detected scattered radiation in the 200-1800 cm^{-1}.

The limits of detection of a CWA simulant in heavily colored liquids were studied by OFC Raman. Triethyl phosphate (TEP) is commonly used as a simulant of Soman (GD), a nerve agent. Fig. 16a presents the spectra of different flavors of Gatorade. The spectra were obtained at the same conditions. Fruit punch presents a higher baseline associated to endogenous fluorescence. TEP was prepared in random concentration from 0 to 100% (V/V). Then the region from 675-855 cm^{-1} was integrated (Fig. 16b). This region was selected because of the presence of the characteristic peaks for phosphates. This region will be the same for the real CWA and related simulants.

Measurements were taken in triplicates from 0 to 100%. Fig. 16c presents average peak areas as a function of TEP concentration in the highly colored solutions concentration. The objective of these graphs is to compare the limit of detection (LOD) and the limit of quantification (LOQ) between colored liquids. Error bars for each data point represent the calculated standard deviation derived from all repetitive measurements each.

Gatorade flavor	LOD (%)	LOQ (%)
fruit punch	6	21
lemon	9	30
orange	9	32

Table 8. LOD and LOQ for TEP in highly colored Gatorade liquids.

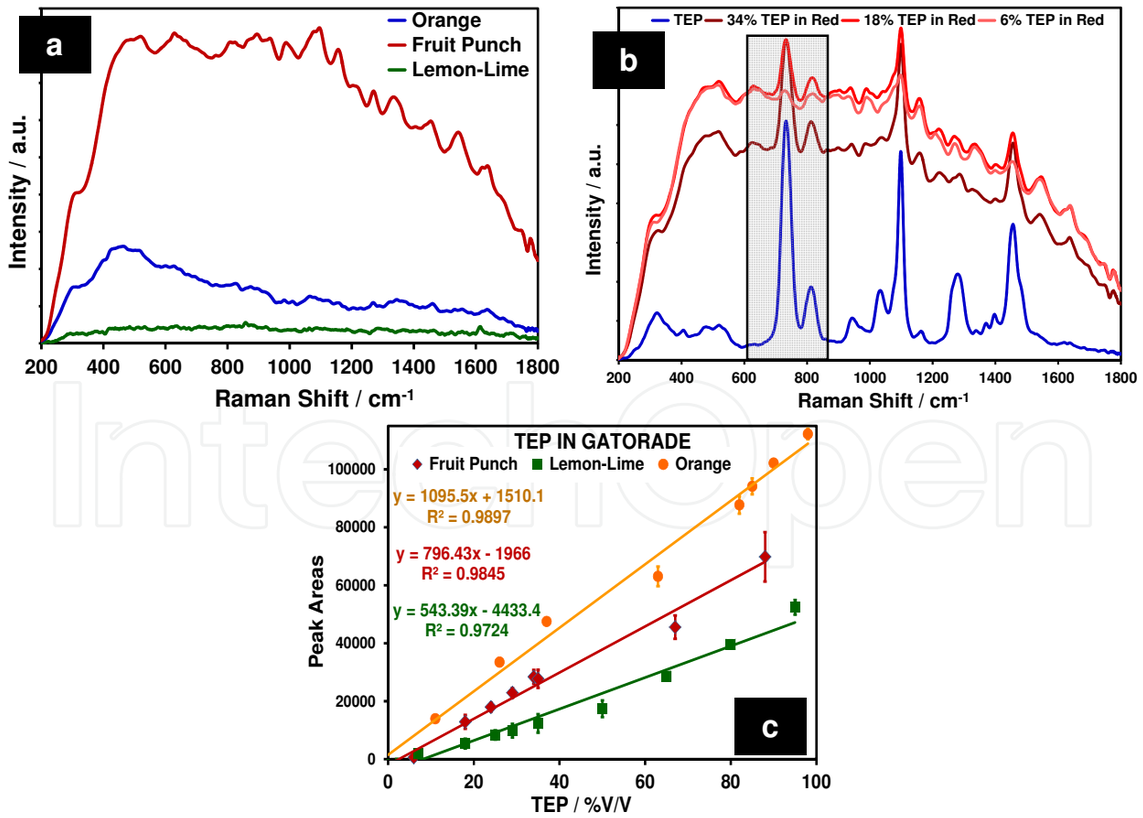

Fig. 16. (a) Raman spectra of Gatorade lemon, orange and fruit punch. (b) Spectrum of neat triethylphosphonate. (c) Peak areas vs. TEP content in the highly colored solutions.

Limits of detection for this analyte have been calculated according to IUPAC by the 3σ criteria (3 times standard deviation of the peak-to-peak noise related to the slope of the linear regression function). When the signal is 3 times as great as the noise, it is ready detectable but still too small for accurate measurement. A signal that is 10 times as great as the noise is defined as the lower limit of quantification (LOQ), or the smallest amount that can be measured with reasonable accuracy. Table 8 presents the results of LOD and LOQ for TEP in Gatorade lemon, orange and fruit punch.

A 488 nm OFC Raman probe was designed, built and tested in quantification of CWA simulants camouflaged as consumer beverages such as purified water and energy drinks.

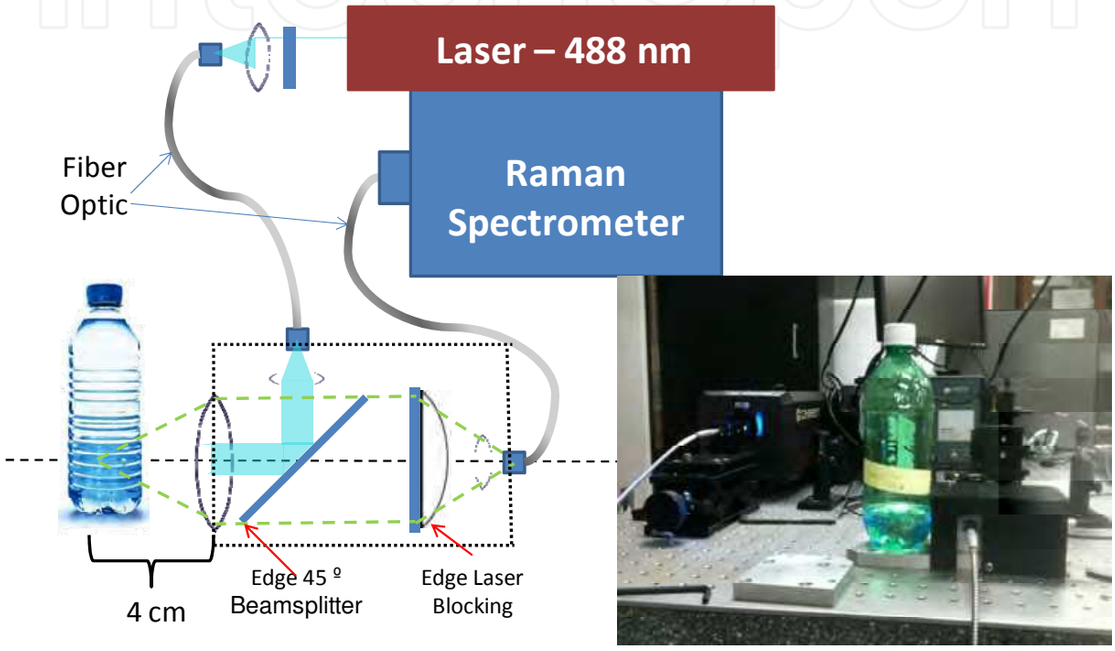

Fig. 17. Optical fiber coupled Raman probe for excitation at 488 nm. Interface to spectrograph was also done with OFC.

Raman experiments were performed using the strong blue line of an argon ion laser INNOVA 310/8 from Coherent, Inc. at 488.0 nm.A single strand optical fiber (non-imaging, 600 µm diameter, model AL 1217, Ocean Optics, Inc.) was used to couple the Raman probe to which a set of laser line filter (to clean satellite lines) and Semrock RazorEdge™ edge filter was used to filter the Rayleigh scattered light. An Andor Technologies spectrograph: Shamrock SR-303i (aperture: f/4; focal length: 303 mm; wavelength resolution: 0.1 nm or 4.2 cm^{-1} at the excitation wavelength) equipped with a 1200 grooves/mm grating was used to analize the Stokes scattered light. A high performance, back thin illuminated CCD camera (Andor Technologies model # DU970N-UVB) with quantum efficiencies of 90% (200 cm^{-1}) to 95% (3200 cm^{-1}) served as light detector. The probe was designed as a combination of two edge filters: the first works at 45° and acts as a mirror for 488.0 nm light, blocking the backscattered Rayleigh light. The second is an edge filter laser blocking at 0° and blocks of remains of the Rayleigh light and transmits the Stokes component of the inelatically scattered signal. The laser light was guided to the probe by optical fiber and the Stoke Raman signal was also transmitted to the spectrometer by optical fibers. A 4 cm focal length

lens focuses the laser light onto of the interior of the plastic/glass bottles. This makes the signal produced at the wall of the bottle minimal.

Four different bottles: clear glass, green glass, brown glass and plastic were used for measure signal Raman of simulant within the container. The simulant used was TEP. Mixtures of simulant and water were used for check the limit of detection. Fig. 18a shows typical OFC Raman spectra of TEP solutions in plastic bottles excited by 488.0 Ar+ line. The calibration curves were obtained by using partial least squares (PLS) regression algorithm of chemometrics and two models were generated. The first model used no preprocessing and the entire spectral region available. For the second model, selected spectral regions were picked by an optimization method, until the best preprocessing was achieved. The optimal regions are shown in Fig. 18b. The optimal preprocessing was vector normalization.

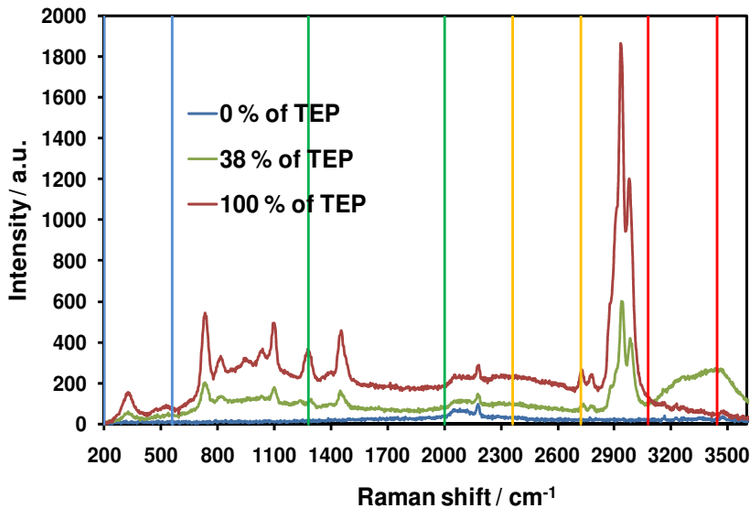

(a)

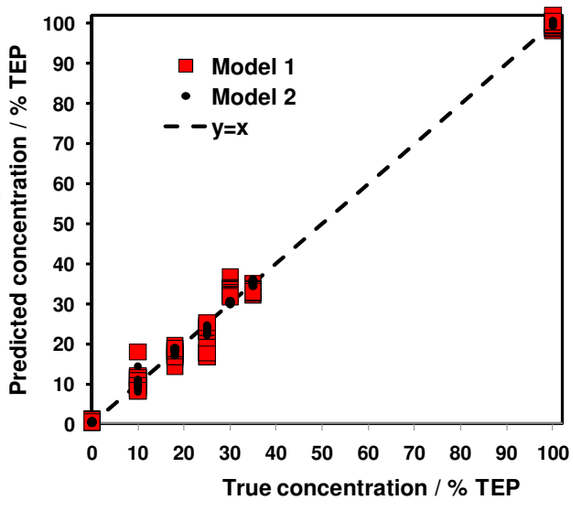

(b)

Fig. 18. (a) OFC Raman spectra of TEP solutions contained in plastic bottles and excited by 488.0 laser line. (b) Predicted vs. true concentrations of TEP in aqueous solutions.

Results of the analysis of the experiments are summarized in Table 9. Both models generated worked well for predicting the TEM concentration, with slightly improved results when vector normalization was applied to the data and individual spectral windows were used instead of the complete spectral range. As can be inferred from Table 9 and using LOD values calculated as 3.3xRMSECV, the detection limit for the model 1 was 7% and for the model 2 was 3%.

	Model 1	**Model 2**
Region (cm^{-1})	3600-199	3441.5-3080.2; 2721.3-2360; 2001-1278.5; 560.5-199.2
Preprocessing	none	Vector normalization
R^2	99.87	99.91
R^2CV	99.32	99.88
RMSEE	1.14	0.914
RMSECV	2.48	1.03
Rank	6	5

Table 9. Summary of statistical inferences for the two methods of analysis of OFC Raman spectral data of TEP solutions.

4. Optical fibers coupled remote raman detection of chemical warfare agents simulants

Chemical warfare agents (CWA) can be classified as weapons of mass destruction (WMD). They include nerve agents, blister agents, choking agents and blood agents. Nerve agents are a group of particularly toxic chemical warfare compounds (Marrs et al., 1996). They were developed just before and during World War II, and they are chemically related to organophosphorus insecticides. The principal compounds in this group are Tabun (GA), Sarin (GB), Soman (GD) and methylphosphonothioic acid (VX). During last two decades, the world has suffered many terrorist attacks that employed chemical warfare agents (CWA) and other hazardous compounds. Examples of such events were seen during the Iran-Iraq war (Henderson, 1999), and in the terrorist attacks in Matsumoto and the Tokyo subway in Japan (Miyaki et al., 2005). These types of terrible events have motivated many countries to focus their defense and security-related research toward the detection of explosives, hazardous liquids and chemical agents that can be used by terrorist organizations as WMD threats against troops or civilians. The anticipation of future attacks requires a wide array of detection systems for a variety of potential deployment scenarios (Sun et al., 2005; Farquharson et al., 2005). There is a need for more sensitive and selective remote detection techniques for chemical threat compounds operating at ambient conditions *in situ* and on a realistic time scale. Remote Raman Spectroscopy (RRS) provides a method for identifying chemicals in samples located meters from the excitation source. In fact, telescope-based Raman spectroscopy detection methods have been reported for standoff detection of chemicals using both visible and UV laser excitation (Hirschfeld, 1974; Angel et al., 1992; Wu et al., 2000; Sedlacek et al., 2001; Sharma et al., 2002; Thomson and Batchelder, 2002; Sharma et al., 2003; Sharma et al, 2005; Pacheco-Londoño et al., 2009; Ramírez-Cedeño et al, 2010).

Recently, our group has applied Remote Raman and Infrared detection systems to the detection and quantification of military high explosives (HEs) and homemade explosives: HME (Pacheco-Londoño et al., 2009) and also the remote detection of hazardous liquids concealed in commercial products bottles (Ramírez-Cedeño et al, 2010). In this manuscript, we report on the design, assembly and testing of two RRS Systems: one operating with continuous wave (CW) laser lines and the other using a pulsed laser system. The collector telescope was modified to operate with both visible (400 - 700 nm) and near-ultraviolet (NUV: 200 - 400 nm) excitation sources for use in the detection of CWAS: dimethyl methylphosphonate (DMMP), 2-chloroethylethylsulfide (2-CEES) and 2-(butylamino)-ethanethiol (2-BAET). Raman scattering cross sections of the studied CWAS were measured using VIS and NUV excitation lines.

The remote-sensing spectroscopic system was also used to detect toxic industrial compounds (TICs): benzene, chlorobenzene, toluene, carbon tetrachloride, cyclohexane and carbon disulfide. The experiments utilizing this remote system used excitation laser lines at 514.5, 488.0, 363.8 and 351.1 nm and a target-collector telescope at a fixed distance of 6.6 m. Further modification of the reflector telescope for use as a receiver allowed for near-field sensing applications at target-collector distances as close as 2.2 m to the target threat liquid chemicals (CWAS and TIC). The visible CW laser excitation system has been described in previous publications (Pacheco-Londoño et al., 2009; Ramírez-Cedeño et al, 2010). Remote Raman measurements of TIC, which are typically strong inelastic scatterers, were initially carried out using this system without any modifications at a fixed target-collector distance of 6.6 m with visible light excitation. In order to measure remote Raman spectra in the NUV and to measure at closer target-collector distances, several modifications had to be made to the receiver reflector telescope. The modified experimental setup for the prototype RRS-based system is shown schematically in Fig. 17. The spectroscopic analysis system consisted of an Andor Technologies Shamrock SR-303i spectrograph, which was equipped with a high quantum response charge-coupled device detector (CCD, Andor Technologies model Newton™ DU-970N-UVB), the appropriate filters for the rejection of satellite plasma lines (laser line filters), and a laser radiation filter designed to block Rayleigh scattered light (edge filters, obtained from Semrock, Inc. Rochester, NY). The nominal detector efficiencies were 95% (532-570 nm), 93% (514.5 nm), 90% (488 nm) and 35% (350-390 nm).

The other necessary components were a reflective telescope used as a collector or signal receiver, a optical fiber assembly, and a single-line laser system operating at 351.1, 363.8, 488.0, 514.5 and 532 nm (Coherent INNOVA 308, Coherent SABRE 25/7 argon ion laser systems; Coherent VERDI-5 solid state diode laser system). The telescope used was a MEADE ETX-125 Maksutov-Cassegrain design (125 mm clear aperture, 1900 mm focal length f /15). The reflecting collector was coupled to the Raman spectrometer with a non-imaging, 600 μm diameter optical fiber (model AL 1217, Ocean Optics, Inc., Dunedin, FL). Two lenses were used to collimate the light from the telescope output, from which the focusing objective was removed, and direct it into the fiber optic assembly. The output of the fiber optic assembly was directly coupled to the Raman spectrometer entrance slit.

The telescope used in the remote detection system was obtained from the manufacturer as a reflective receiver operating in the VIS region only. It was modified to allow for the collection of scattered Raman signals in the near-ultraviolet region, 350-390 nm, by coating the secondary mirror with a thin layer (~ 200 nm) of UV-reflective aluminum. In addition, the minimum focal point where a clear image could be formed was 5 m. An anodized

aluminum tube with capabilities of rigidly holding two quartz lenses and moving the lenses to change the focal distance was integrated to the beam path to allow for a reduction of the minimum focal point to 2.0 m adding near-field proximity detection capability. The system was successfully tested at a 2.2 m target-collector distance. Although RRS spectra are not shown, data is but included as part of system performance tests. The changes made to the collector telescope are also illustrated in Fig. 19.

The pulsed laser standoff Raman system used the components of the CW system with the exception of the excitation source and the spectrometer detector. A frequency-doubled 532 nm Nd:YAG pulsed laser system (Quanta Ray INDI Series, Newport-Spectra Physics, Mountain View, CA) was used as the excitation source. The maximum energy/pulse of the laser at 532 nm was 200 mJ, and it operated at a repetition rate of 10 Hz. The pulse width was approximately 5-8 ns, and the beam divergence was less than 0.5 mrad. A gateable, intensified CCD detector (iStar™ ICCD camera, Model DH-720i-25F-03, Andor Technology, Belfast, Northern Ireland) was used as the photon detector. Andor Technology Solis™ software for spectroscopic, imaging and time-resolved studies was used for spectral data acquisition and processing from the intensified and gated CCD detector. Using this software, the data could be acquired in both imaging and spectroscopic modes.

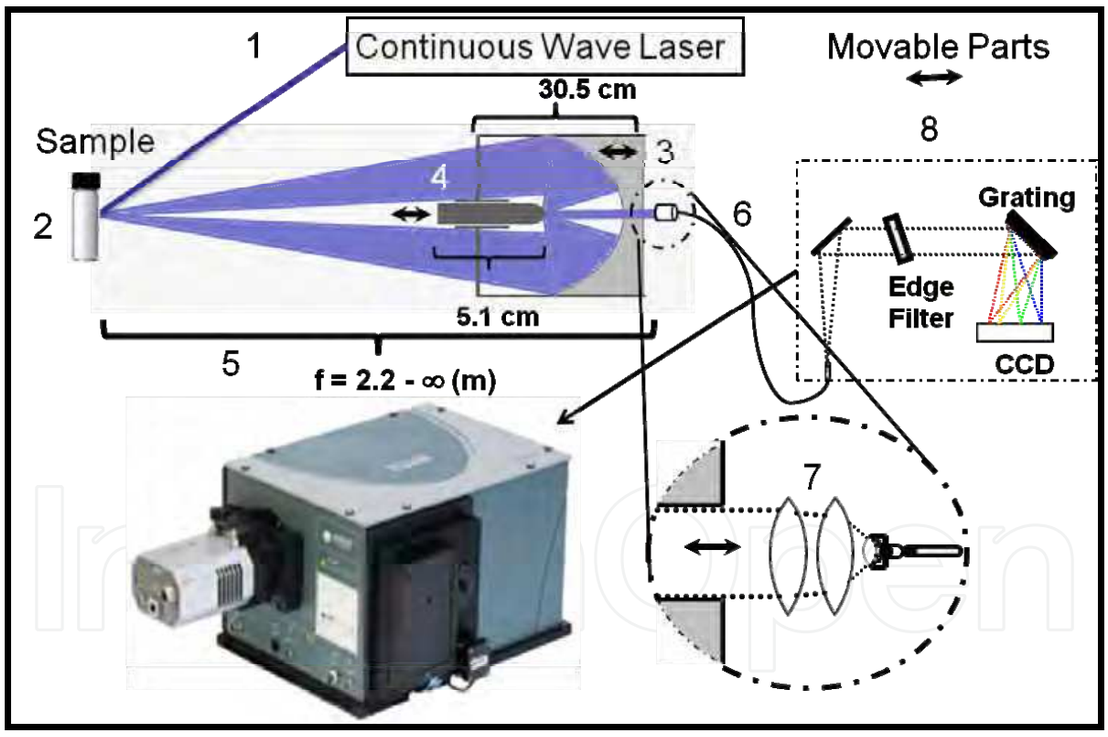

Fig. 19. Design details of the Remote Raman Detection System: (1) laser source; (2) sample; (3) reflective telescope signal collector; (4) variable focus secondary mirror; (5) standoff distance; (6) fiber optic coupling; (7) details of optical coupling; (8) spectrograph. Movable optical elements are represented by double head arrows.

The remote system was tested using TIC and CWAS. The toxic industrial compounds investigated were chlorobenzene, toluene benzene, carbon disulfide, carbon tetrachloride and cyclohexane (all from Fisher Scientific International, Chicago, IL). The chemical warfare

agents simulants (CWAS) studied were dimethylmethyl phosphonate (DMMP, 99%, Fisher Scientific International, Chicago, IL), 2-chloroethyl ethyl sulfide (2-CEES, Sigma Aldrich Chemical Company, St. Louis, MO), and 2-(butylamino)-ethanethiol (2-BAET, Sigma-Aldrich). For CW remote detection experiments, pure liquid samples were transferred to 5 mL glass or quartz vials and placed 6.6 m away from the receiver telescope/excitation laser. The spectra of all compounds were collected with the laboratory lights off to avoid background light and mercury lines from fluorescent lamps. The spectra were acquired in the Raman Shift range of 100-1800 cm^{-1} at laser powers (measured at head) ranging from 0.05 to 1 W and a single acquisition with integration time of 1-30 s. Quantification studies of DMMP/water solutions were carried out at a fixed 6.6 m target-collector distance using the CW RRS system only.

Standoff detection experiments on DMMP at 35 m and cyclohexane at 60, 90 and 141 m were carried out using pulsed mode laser RRS system. DMMP was contained in clear glass bottles 2.5 cm in diameter and 5.0 cm high. For acquisition of remote Raman spectra of cyclohexane at the longest distances, the sample was contained in clear glass bottles that were 7.5 cm in diameter and 15.2 cm high. The criterion used for changing vials at longer distances was that the beam diameter at the sample would be smaller than the cross section of the vials containing the samples. Liquids were remotely detected in the spectroscopic range of 500 to 3200 cm^{-1} using 1 to 1000 pulses of 532 nm excitation wavelength, with pulse energy of ~ 200 mJ.

Important industrial solvents and starting materials used for manufacturing in the petrochemical, pharmaceutical, electronic, and other chemical industries are highly flammable, lachrymatory, toxic, mutagenic or carcinogenic. Some of these compounds are used in amounts that constitute potential threats. Thus, it is vital to find ways of monitoring these compounds in air and in their container bottles. Remote Raman systems offer new and simple alternatives to carry out these monitoring processes by remote sensing of the liquid and even the vapor phase (UV Raman). Figures 2 and 3 illustrate the remote CW Raman spectra of organic solvents, some of which are constituents of hydrocarbons found in petroleum-processing plants. All of the spectra were collected at a distance of 6.6 m from the telescope under laboratory conditions using low illumination. Samples were detected using 514.5 nm laser line excitation at 1W (measured at head) using a single acquisition and integration time of 10 s.

The most prominent feature common among all the spectra in Fig. 20a is the aromatic ring-breathing mode at ca. 1000 cm^{-1}. This strong Raman band is characteristic of the symmetric stretch mode of the benzene ring at 992 cm^{-1} (Lin Vien et al, 1991; Shrader, 1995; McCreery, 2000). In the case of toluene and chlorobenzene, the same band appeared at 1003 cm^{-1}. Another characteristic band of toluene was found at 786 cm^{-1}. The C-Cl stretching mode of chlorobenzene was clearly observed at about 700 cm^{-1} in the Raman Shift spectrum of this TIC.

Several organic solvents widely used in industry, teaching, and research labs were also studied. Among these solvents were carbon disulfide, carbon tetrachloride and cyclohexane. Typical Remote Raman spectra are shown in Fig 20b. All of these compounds have characteristic physical and chemical properties. Cyclohexane is typically used as a calibration standard for the Raman Shift axis in dispersive instruments, particularly in Raman studies of liquids (Evans and Bernstein, 1956). In this work, the Remote Raman spectra of these compounds were measured for liquids contained in 5 mL clear glass vials in the 150–1800 cm^{-1} range at a standoff distance of 6.6 m (Fig. 20b).

In Fig. 20b, it is possible to identify carbon disulfide by its very strong (highly symmetric nature) peak at ca. 655 cm^{-1}, corresponding to the C-S symmetric stretching mode (Wakabayashi et al., 2007). Carbon tetrachloride shows its three main Raman active peaks. The most important band for CCl_4 appears at 461 cm^{-1}. This band is attributed to C-Cl symmetric stretching mode (Crain et al., 1992). According to the literature, cyclohexane is characterized by four prominent bands in the 800-1650 cm^{-1} region: a very strong peak at 801 cm^{-1} due to the C–C skeletal breathing mode, the weak peak localized at 1029 corresponds to C–C stretching modes, and other, weak peaks that appear at 1260 and 1445 cm^{-1} due to twisting and scissoring modes (Evans and Bernstein, 1956; Sharma, 2007).
The continuous wave (CW) standoff Raman system was originally designed to measure Raman Shift spectra excited at visible light frequencies (514.5 and 488.0 nm) at a fixed remote distance of 6.6 m. This was based on two main factors: maximum standoff distance due to restrictions based on laboratory space and minimum focal distance of the visible wavelength reflective telescope used as receiver. After successful measurements under the original operating conditions of HE, HME [14] and TICs (the present study), the system was switched operate in the near-ultraviolet region (NUV), and the signal receiver (telescope) was modified to operate as a close field (proximity) detector (1-2 m). After making the necessary changes, the remote detection system was subjected to the challenging task of detecting extremely low cross-section liquids: CWASs.

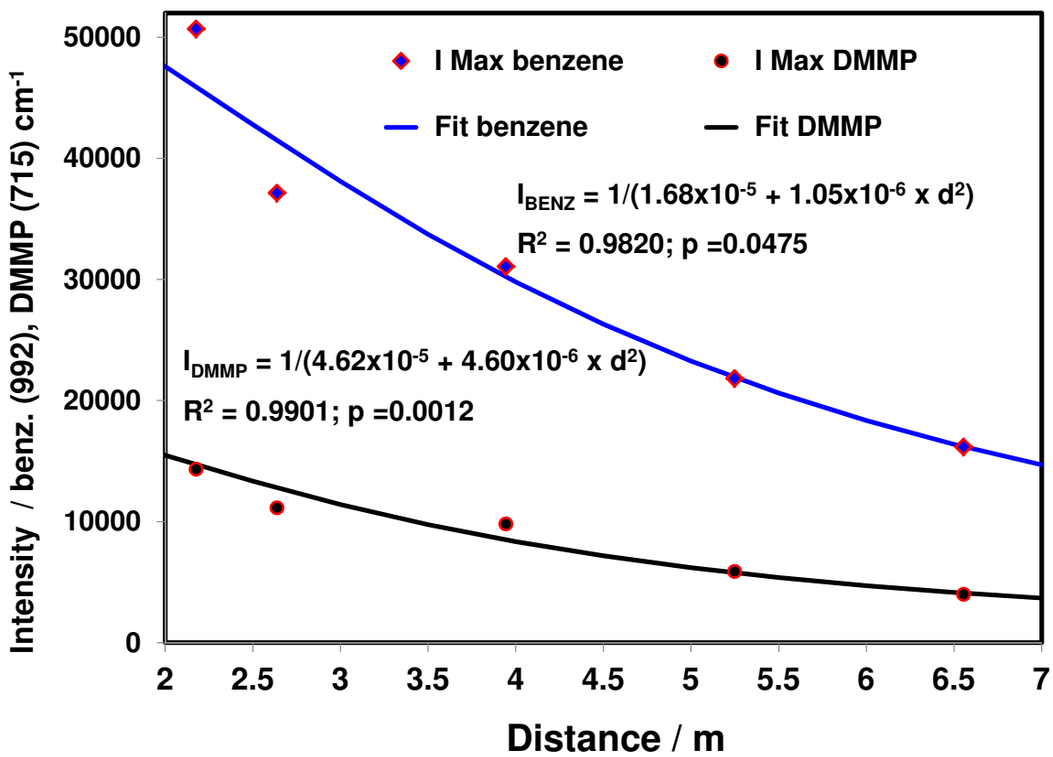

Fig. 20. Dependence of Raman Shift signal (vibrational band intensities) with standoff distance for benzene and DMMP using the 363.8 nm excitation line from a UV-argon ion laser.

Fig. 21 shows results of the remote detection system for the intensities of the Raman bands of benzene (ring breathing mode at 992 cm^{-1}) and DMMP (C-P stretch at 715 cm^{-1}) at various distances from 2 to 7 m using a CW argon ion laser excitation line at 363.8 nm. The dependence of the band intensities for the most prominent signals of benzene (used as primary external standard) and DMMP were plotted and then a line was fitted to the data as a function of the target-receiver distance using Statgraphics-Centurion™ data analysis and statistical software package (StatPoint, Inc., Herndon, VA). The resulting fits, shown in Figure 4, were non-linear, as expected, and compared favorably with the data.

The decrease of the Raman intensity of the benzene and DMMP peaks with increasing distance is partially attributed to the $1/R^2$ dependence of the remote Raman signal with standoff distance. However, the signal losses are also related to near-field effects and to partial defocusing of the image on the slit of the spectrograph (Chistesen, 1988). The current version of the CW laser remote spectroscopic system is probably less able to detect very long source-target distances (standoff distances) compared to pulsed laser systems because of the higher energy densities in the beam axis of the pulsed systems. However, at close range, working as a near field detector, the CW standoff Raman detection system works equal or better than the pulsed system. The following two cases will provide experimental evidence for this supposition.

Remote Raman spectra were excited using uncollimated CW and pulsed laser beams. Laser power levels of CW lasers were 0.140 to 5.1 W. The calculated values for energy/area taking into account the laser beams spot size at the sample were 1.5 to 8.3 W/cm^2 (1.5 – 8.3 W/cm^3 energy densities for a sample vial 1-cm in diam). For the pulsed laser experiments, up to 1000 pulses of 200 mJ/pulse (6 ns, 10 Hz) were used, resulting in a maximum average power of 2.0 W. At a standoff distance of 6.6 m, the pulsed laser spot was an ellipse with a major semi-axis of 2.5 cm and minor semi-axis of 1.5 cm. This corresponds to an energy/area of 0.68 W/cm^2 (0.68 W/cm^3 in a 1-cm diam. vial) or roughly 47% of the minimum value for the steady-state detection system. Table 10 lists the relevant laser beam characteristics of the standoff system. In contrast, typical normal or spontaneous Raman measurements under the microscope use power density values on the order of 12,500 W/cm^3 to excite the Raman Shift spectra of samples contained in capillary tubes (100 mW, 10x objective, 10 μm spot size in confocal mode, $8x10^{-6}$ cm^3 interrogation volume). This represents a 1,500 to 8,000-fold higher energy density value for the microscope experiments than the telescope-based CW Raman experiments. Raman scattering cross sections, $(d\sigma/d\Omega)_s$, of CWAS were calculated by performing intensity measurements and relating them according to the treatment of Christesen (1988) via Eq. 1:

$$\frac{\left(\frac{d\sigma}{d\Omega}\right)_s}{\left(\frac{d\sigma}{d\Omega}\right)_r} = \frac{A_s\ N_s\ n_s\ E_s}{A_r\ N_r\ n_r\ E_r} \tag{1}$$

In the above equation, the subscripts s and r indicate the CWAS and reference values, respectively. A_s and A_r are the sample and reference integrated peak areas, which was measured from the spectra, and N_i is the number of molecules per unit volume, which was obtained from the sample and reference densities. The collection solid angle of the

spectrometer is a function of the index of refraction of the liquid (n_i) and was accounted for by the ratio (n_s/n_r). E_i is an instrument efficiency factor that depends on the wavelength of the scattered light. If the sample and reference bands are close together (as they are typically chosen) the ratio E_s/E_r can be taken as 1. An additional factor would be necessary in Eq. 1 if either the sample or reference absorb at the laser wavelength (Christesen, 1988).

λ (nm)	Spot Diam. at 6.6 m (cm)	Area (cm^2)	Laser Power (Energy) (W / mJ)	Energy/Area (W/cm^2)
532.0 (CW)	1.0	0.79	5.10	6.49
514.5	0.4	0.13	1.00	7.96
488.0	0.4	0.13	1.00	7.96
363.8	0.35	0.10	0.80	8.32
351.1	0.35	0.10	0.14	1.46
532.0 (pulsed)	2.5x1.5*	2.95	2.00 / 200	0.68

* spot is elliptical in shape

Table 10. Remote Raman spectroscopy systems laser beams characteristics.

This method was applied to a comparison between the most prominent Raman band of the CWAS and the 992 cm^{-1} band of benzene and/or the 801 cm^{-1} band of cyclohexane. Benzene and cyclohexane were chosen as references (external primary standards). The cross-section data for the CWAS and reference compounds studied are shown in Table 11. These compounds are relatively weak Raman scatterers in comparison to the reference compounds. For this reason, the standoff detection of CWAS was an important instrument challenge, as suggested by Christesen (Christesen, 1988).
The Remote Raman spectra of three CWASs: 2-BAET, 2-CEES and DMMP, are shown in Fig. 21. All spectra were collected in the visible and NUV at a distance of 6.6 m from the collector telescope. The samples were detected using the strong blue line of the argon ion laser at 488.0 nm and NUV lines at 363.8 and 351.1 nm with 1 W laser power (at head) and a spectral acquisition time of 10 s. Raman peaks at 660 and 1440 cm^{-1} were tentatively assigned to C-S and C-N stretching vibrations, respectively, for the 2-BAET simulant (Fig. 21, top). A strong line appearing at about 700 cm^{-1} was tentatively assigned to C-Cl in 2-CEES (Fig. 5, center). Raman signals located about 660 and 750 cm^{-1} were attributed to the C-S and C-S-C of this simulant, respectively. The peak at 715 cm^{-1} for DMMP (Fig. 21, bottom trace) was assigned to a P-C stretching mode.

	Cross Sections (10^{-30} cm^2/sr/molecule)				
Exc. line (nm)	benzene (992 cm^{-1})	cyclohexane (801 cm^{-1})	DMMP (715 cm^{-1})	2-CEES (700 cm^{-1})	2-BAET (1440 cm^{-1})
532.0	13.4 [c]	3.6	3.7	2.8	2.7
488.0	32.5 [c]	9.06 [b]	18.0 [a]	15.1	20.3
363.8	328.4	105.6	58.0 [a]	21.4	10.3
351.1	160.0 [b]		17.2	5.4	3.3

Data adapted from: a ~ (Evans and Bernstein, 1956); b ~ (Wakabayashi et al., 2007); c ~ (Crain et al., 1992).

Table 11. Relative differential Raman scattering cross sections.

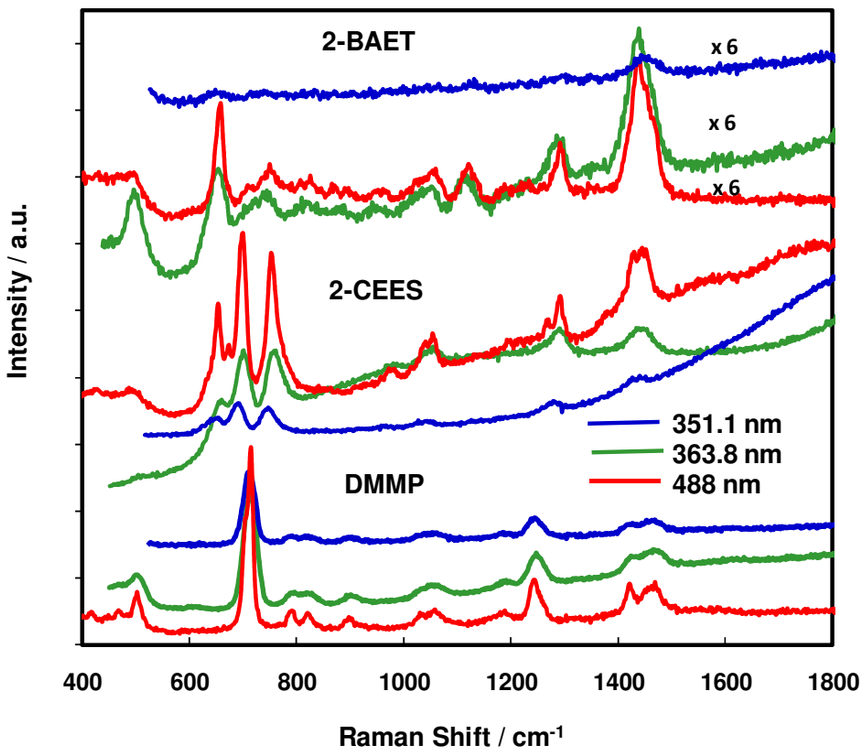

Fig. 21. Remote Raman spectra of CWAS using excitation lines of 488.0, 363.8 and 351.1 nm at 6.6 m target-collector distance, 1 W laser power (at head) and one acquisition time of 10 s integration. Top: 2-(butylamino)-ethanethiol (2-BAET); center: 2-chloroethyl-ethyl sulfide (2-CEES); bottom: dimethylmethyl phosphonate (DMMP).

Pulsed laser Standoff Raman spectra of cyclohexane and DMMP in the spectral range 500 - 3200 cm^{-1} are shown in Figs. 22a and 22b. The measurements were collected at distances of 35 m (DMMP) and 60, 90 and 141 m (cyclohexane) with gated detection using several 532 nm laser pulses (from 1 to 1000 shots) with 200 mJ per pulse. These experiments were performed under "lights on" conditions. The most relevant spectroscopic information for both compounds was presented in the CW laser excitation section. Pulsed mode experiments (Figs. 6 and 7) were obtained using the ICCD camera, which was gated and synchronized with laser pulses to minimize interference from ambient light. The cyclohexane RRS spectra at 60 m and 90 m standoff distances were nearly identical. This similarity was the result of a size beam smaller that the target at both distances. However, the beam diameter at 141 m was significantly larger than the sample, which resulted in a reduced energy density and a lower scattering signal. However, even operating under these conditions, the cyclohexane spectrum at 141 m obtained with 1000 laser pulses had a good signal-to-noise ratio (S/N = 450). The S/N value was determined by dividing the highest intensity Raman band of cyclohexane by the Root-Mean-Square (RMS) noise, calculated by taking a portion of the flattest region of the cyclohexane spectrum (1900-2100 cm^{-1}). Both

compounds can be detected with a single laser shot, but S/N became statistically significant by averaging the intensity collected after 10 laser shots, as can be seen in Fig. 22a. It is important to note the advantages of a pulsed laser system over CW systems for Raman detection at a distance. When operating in a gated detection mode, the background light signal and fluorescence signal are significantly reduced. Because the detector is acquiring for 400 ns, the fluorescence contributions that dominate at a longer time scale (~ μs) are minimized. One of the main disadvantages of the CW Remote Raman detection system is the necessity of operating under low-illumination conditions. This problem can be readily circumvented by using a gated Intensified-Charge Coupled Device (I-CCD), UV-VIS-capable detector.

An even more challenging application for the standoff Raman spectroscopy detection system was to perform quantification studies of a weak Raman scatterer mixed to less than 10% dilution with water. This task was undertaken using DMMP. In order to carry out the quantification experiments on DMMP, water, solutions of the analyte ranging from 1 to 50 % w/v were prepared and analyzed using CW RRS. For the quantification studies, peak areas of the strongest DMMP Raman signal located about 715 cm^{-1} were used (Fig. 8).

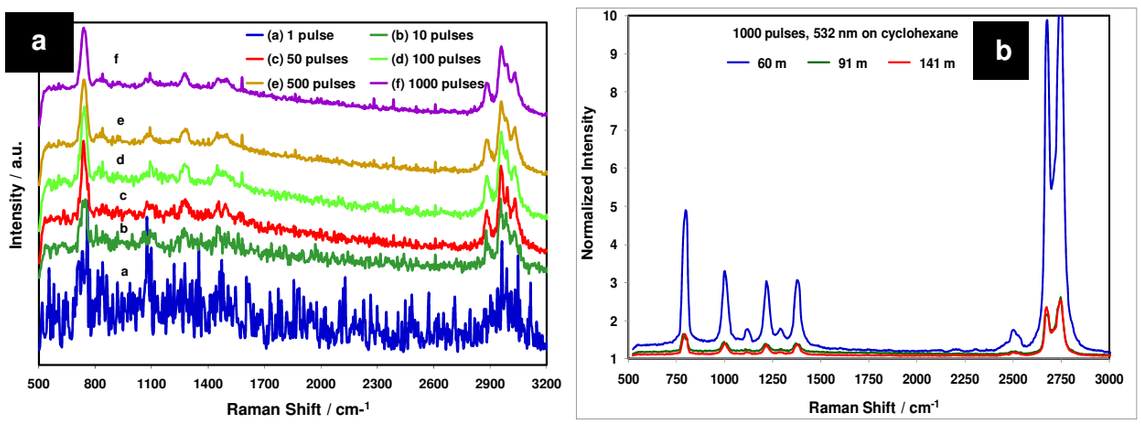

Fig. 22. Left: Remote Raman spectra of DMMP using a 532 nm pulsed laser excitation source at a distance of 35 m, measured with various laser shots in gated mode. Laser: 532 nm, 200 mJ/pulse, 10 Hz. Right: Remote Raman spectra of cyclohexane using a 532 nm pulse laser at standoff distances of 60, 90 and 141 m, measured with 1000 laser shots in gated mode. Laser: 532 nm, 200 mJ/pulse, 10 Hz; gate width 400 ns.

5. Conclusion

In this contribution, TIJ and sample smearing were used as deposition methods for the preparation of samples and standards of highly energetic materials deposited as solid traces onto gold coated silicon substrates. Inkjet printing of HEM was demonstrated to have the following important characteristics: precision in sample deposition, drop delivery with non-contact fluid transfer and high reproducibility. These characteristics led to the production of evenly distributed analytes on the test surfaces. The methodology promises to be a good method for development of samples and standards for trace HEM

reference materials on substrates. Sample smearing, a technique that had been proven successful for similar operations on stainless steel, glass and plastics, although easy to implement and of inherently low cost, yielded very poor yields on the gold on silicon substrate because of weak interactions between the analytes studied and the test surfaces. Gold coated silicon is probably an excellent test surface for IR reflection studies, but it lacks the sample adhesion forces required to deposit and retain analytes for long enough periods of time to be of value in samples and standards preparation. The residence time of TNT on gold coated silicon was twice as short as TNT on glass and four times shorter than TNT on a stainless steel substrate.

Both methods demanded relatively long preparation and analysis times, depending on the specific sample and substrate requirements, and thus neither methodology stands out as superior from these points of view. Sample deposition by smearing requires higher human intervention, both in the pre-deposition steps and in the actual smearing operation. TIJ requires minimal operator intervention. Deposition by TIJ is a more efficient process than smearing with regard to ease of use, fine control of the amount deposited and the surface loadings achieved. The actual amounts deposited (loadings) had to be determined post-deposition by destructive chemical analysis. This is in contrast to sample smearing deposition, for which the amount deposited is accurately known except in cases of insufficient adhesion such as with gold coated substrates.

The loading concentrations of the highly energetic materials studied (TNT, RDX and ammonium nitrate) were varied by changing the number of passes of the TIJ dispenser. TIJ samples and standards were deposited onto three surfaces, gold-silicon, glass and SS, for surface comparison experiments. Studies are required when searching for substances that stabilize the analytes on the substrate by delaying sample loss through sublimation, which would ultimately interfere with detection applications. The characteristics of the stabilizing agent must not alter or mask the activity and reactivity of the energetic materials with respect to the detection applications.

A standoff technique using an open-path Fourier transform infrared (OP/FTIR) spectrometer has been demonstrated in In another contribution, concealed liquids scenarios are studied by Raman spectroscopy. The Raman spectra of hazardous liquids were differentiated from common drinks and consumer products. A fiber optic coupled Raman probe was applied to the detection of hazardous liquids mixed with consumer products and drinks. The results demonstrated that Raman can be used as tool to quickly characterize if the content of a bottle is the intended commercial product or a hazardous liquid that could be used as a threat to property or human beings. The fluorescence of a red liquid did not affect the detection of a CWA simulant in a clear glass container. The limits of detection for a hazardous liquid in a series of colored liquids were estimated in 6-9 % using standard conditions and no data manipulation. This suggests that trace level detection can be achieved with enhanced experimental setups and statistical analysis of the data (chemometrics).

In the third application of optical fibers in spectroscopy, remote Raman systems have been designed, assembled and tested by coupling a Raman spectrometer with a reflective telescope using fiber optics. The CW RRS system employed 351.1, 363.8, 488.0, 514.5 and 532 nm continuous wave lasers as excitation sources. This prototype system

was used in the detection of the chemical warfare agent simulants DMMP, 2-CEES and 2-BAET, and to detect the hazardous industrial solvents and reagents (TICs) benzene, toluene, chlorobenzene, carbon disulfide, carbon tetrachloride and cyclohexane. The operational range of the CW standoff system was tested up to 6.6 m in the laboratory with no background illumination. In addition, quantification studies of DMMP in water were carried out at a standoff distance of 6.6 m using the CW remote Raman detection system. Low limits of detection (LOD) values of 3% w/v were consistently obtained. The pulsed mode RRS system was based on a 532 nm, frequency doubled Nd:YAG laser in lieu the CW excitation lasers of allowed standoff detection experiments of DMMP at 35 m target-collector distances, from single shot to 1000 shots and also allowed detection of cyclohexane at 141 m standoff distance even in single shot mode. The Remote Raman Spectroscopy systems designed in this work should be useful for defense and security applications, for screening hazardous liquids in government installations, airports and seaports and in public installations to improve defense against terrorist attacks.

6. Acknowledgments

Parts of the work presented in this contribution were supported by the U.S. Department of Defense, University Research Initiative Multidisciplinary University Research Initiative (URI)-MURI Program, under grant number **DAAD19-02-1-0257**. The authors also acknowledge contributions from Mr. Aaron LaPointe from Night Vision and Electronic Sensors Directorate, Fort Belvoir, VA, Department of Defense, Dr. Jennifer Becker MURI Program Manager, Army Research Office, DoD and Dr. Stephen J. Lee Chief Scientist, Science and Technology, Office of the Director, Army Research Office/Army Research Laboratory, DoD.

Support from the U.S. Department of Homeland Security under Award Number **2008-ST-061-ED0001** is also acknowledged. However, the views and conclusions contained in this document are those of the authors and should not be interpreted as necessarily representing the official policies, either expressed or implied, of the U.S. Department of Homeland Security.

The authors want to acknowledge graduate and undergraduate students from the Departments of Chemistry, Chemical Engineering and Biology for participating in several of the stages of this project. Support personnel from the Department of Chemistry are also gratefully acknowledged, including Aracelis Cardona, Cynthia Ramos, Cacimar Ramos and Rosalie Ramos.

7. References

Allain, L.R., Stratis-Cullum, D.N., Vo-Dinh, T. (2004). Investigation of microfabrication of biological sample arrays using piezoelectric and bubble-jet printing technologies. *Anal. Chim. Acta*, 518 (1-2), 77-85.

Alvarez-Rivera, M. (2002). Fiber Optic Coupled Raman Spectroscopy of liquid explosives mixtures. University of Puerto Rico, Mayaguez.

Angel, S.M., Kulp, T.J. & Vess, T.M. (1992). Remote-Raman Spectroscopy at Intermediate Ranges Using Low-Power cw Lasers. *Appl. Spectrosc.*, *46*, 1085-1091.

Beeson, R., Skip, R.D., Thermal inkjet technology -review and outlook. Advanced Research Laboratory, Inkjet Business Unit, Hewlett-Packard Company, Corvallis Oregon, US.

Christesen, S. D., (1988). Raman cross sections of chemical agents and simulants. *Appl. Spectrosc., 42*, 318-321.

Christesen, S.; Maciver, B.; Procell, L.; Sorrick, D.; Carrabba, M.; Bello, J., (1999) Nonintrusive Analysis of Chemical Agent Identification Sets Using a Portable Fiber-Optic Raman Spectrometer. *Applied Spectroscopy 53*, 850-855.

Crain, J., Poon, W. C., Cairns-Smith, A., Hatton, P. D., (1992). High-pressure Raman spectroscopic study of cyclohexane C_6H_{12} and C_6D_{12}. *J. Phys. Chem*. 96, 8168 - 8173

D'Agostino, P.A.; Hancock, J.R.; Chenier, C.L.; Lepage, C.R., (2006). Liquid chromatography electrospray tandem mass spectrometric and desorption electrospray ionization tandem mass spectrometric analysis of chemical warfare agents in office media typically collected during a forensic investigation. *J Chromatogr A*, 1110 (1-2), 86-94.

Eliasson, C.; Macleod, N.; Matousek, P., (2007). Noninvasive Detection of Concealed Liquid Explosives Using Raman Spectroscopy. *Analytical Chemistry 79* (21), 8185-8189.

Evans, J. C. and Bernstein, H. J., (1956). The effect of Intermolecular interaction on Raman spectrum of carbon disulphide. *Can. J. Chem.* 54, 1127 – 1133.

Ewing, R.G., Atkinson, D.A., Eiceman, G.A., Ewing, G.J. (2001). A critical review of ion mobility spectrometry for the detection of explosives and explosive related compounds. *Talanta*. 54 (3), 515-529.

Farquharson, S., Gift, A., Maksymiuk, P., (2005). Inscore, F. Surface-enhanced Raman spectra of VX and its hydrolysis products. *Appl. Spectrosc.*, *59*, 654-659.

Fierro-Mercado, P.M., Primera-Pedrozo, O.M., Hornedo, A., Hernández-Rivera, S.P., (2010). An In situ FTIR Fiber Optic Method for the Detection of Active Pharmaceutical Ingredients and Excipients on Metallic Substrates, in "Fourier Transform Infrared Spectroscopy: Developments, Techniques and Applications. Nova Science Publishers, Inc. Hauppauge, NY.

Fletcher, R., Briggs, N., Ferguson, E., Gillen, G., (2008). Measurements of air jet removal efficiencies of spherical particles from cloth and planar surfaces. Aerosol science and technology, 42 (12), 1052-1061.

Gillen, G., Zeissler, C., Mahoney, C., Lindstrom, A., Fletcher, R., Chi, P., Verkouteren, J., Bright, D., Lareau, R.T., Boldman, M. (2004). Automated analysis of organic particles using cluster SIMS. Applied Surface Science, 231-232, 186-190.

Hallowell, S.F. (2001). Screening people for illicit substances: a survey of current portal technology. *Talanta*. 4 (3), 447-458.

Hamilton, M.L.; Perston, B.B.; Harland, P.W.; Williamson, B.E.; Thomson, M.A.; Melling, P.J., (2005). *Organic Process Research & Development*. 9, 337–343.

Harvey, S. D.; Vucelick, M. E.; Lee, R. N.; Wright, B. W., (2002).Blind field test evaluation of Raman spectroscopy as a forensic tool. *Forensic Science International,* 125 12–21.

Heimerl, J.M., (1999). A Forensic Workshop Report Concerning (1) The Measurement and Analysis of Energetic Materials and (2) Databasing. A.R. Laboratory (Ed.), Aberdeen Proving Ground, MD.

Henderson, D.A. (1999). The looming threat of bioterrorism. *Science,* 283, 1279-61282.

Hernández, N.M., Rosario, S.V., Hernandez, S.P., Mina, N., (2005). Detection and characterization of smokeless powders with ion mobility spectrometry. *Proc. SPIE Int. Soc. Opt. Eng.* 5778, 607-616.

Hirschfeld, T., (1974). Range Independence of Signal in Variable Focus Remote Raman Spectrometry. *Appl. Opt*., *13*, 1435-1437.

Irrazabal, M., Florian, V., Castro, M., Hernandez-Rivera, S.P., Briano, J.G., (2007). Effect of environmental parameters on the chemical signature of TNT in soil. *Proc. SPIE Int. Soc. Opt. Eng.* 6553, 65531N-65541N.

Lin-Vien, Colthup, N.B., Fateley, W.G., Grasselli, J.G. (1991). The Handbook of Infrared and Raman Characteristic Frequencies of Infrared and Raman Characteristic Frequencies of Organic Molecules. Academic Press. San Diego, CA.

McCreery, R. L. *Raman Spectroscopy for Chemical Analysis*. (2000). New York, NY: Wiley-Interscience.

MacCrehan, W.A., (2004). Development of a NIST trace particulate explosives Reference material to evaluate IMS detectors National Institute of Standards and Technology, Gaithersburg, MD 20899-8392 USA.

MacCrehan, W.A. (2009). A NIST Standard Reference Material (SRM) to Support the Detection of Trace Explosives. Analytical Chemistry, 81 (17), 7189-7196.

Manrique-Bastidas, C.A., Castillo-Chara, J., Mina, N., Castro, M.E., Hernandez-Rivera, S.P., (2004). Nucleation and crystallization studies: A vibrational spectroscopy investigation of 2,4,6-TNT. *Proc. SPIE Int. Soc. Opt. Eng.* 5415, 1345-1356.

Manrique-Bastidas, C.A., Primera-Pedrozo, O.M., Pacheco-Londono, L., Hernandez-Rivera, S.P., (2004). Raman microspectroscopy crystallization studies of 2,4,6-TNT in different solvents. *Proc. SPIE Int. Soc. Opt. Eng.* 5617, 429-441.

Marrs, T.C. Maynard, R.L. and Sidell, F.R., (1996). Chemical Warfare Agents: Toxicology and Treatment. John Wiley & Sons Ltd., London, UK.

Melling, P.J.; Shelley, P. (2002). Spectroscopic Accessory for Examining Films and Coatings on Solid Surfaces. U.S Patent 6,3,10,348, United States Patent and Trademark Office, Washington, DC.

Mehta, N.K.; Goenaga-Polo, J.E.; Hernández-Rivera, S.P.; Hernández, D.; Thomson, M.A; Melling, P.J., (2002). Development of an *In-Situ* Spectroscopic Method for Cleaning Validation Using Mid-IR Fiber Optics. *Bio Pharm*., 15, 36-42.

Mehta, N.K.; Goenaga-Polo, J.E.; Hernández-Rivera, S.P.; Hernández, D.; Thomson, M.A; Melling, P.J., (2003). Development of an *In-Situ* Spectroscopic Method for Cleaning Validation Using Mid-IR Fiber Optics *Spectroscopy*, April.

Meier, B., Weidner, P. and Penzkofer, A., (1990). Double line stimulated Raman scattering in benzene. *Appl. Phys. B*, *51*, 404-413.

Mocak, J., Bond, A.M., Mitchell, S. and Scollary, G.A. (1997). Statistical overview of standard (IUPAC and ACS) and new procedures for determining the Limits of detection and

quantification: application to voltammetric and stripping techniques. *Pure Appl. Chem., 69*, 297-328.

Miyake, A.; Yamada, N.; Ogawa, T., (2005). Mixing hazard evaluation of organic peroxides with other chemicals. *Journal of Loss Prevention in the Process Industries 18* (4-6), 380-383.

Miyaki, K., Nishiwaki, Y., Maekawa, K., Ogawa, Y., Asukai, N., Yoshimura, K., Etoh, N., Matsumoto, Y., Kikuchi, Y., Kumagai, N. and Omae, K. (2005). Effects of Sarin on the Nervous system of subway workers seven years after the Tokyo subway Sarin attacks. *J. Occup. Health*, *47*, 299-304.

National Research Council. Final Report on Existing and Potential Standoff Explosives Detection Techniques. (2004). Published by the National Academy of Sciences.

Pacheco-Londono, L.C., Santiago, A., Pujols, J., Primera-Pedrozo, O.M., Mattei, A., Ortiz, W., Ruiz, O., Ramirez, M., Hernandez-Rivera, S.P., (2007). Characterization of layers of Tetryl, TNB and HMX on metal surfaces using fiber optics coupled grazing angle-FTIR. *Proc. SPIE Int. Soc. Opt. Eng.* 65423K-65410.

Pacheco-Londoño, L.C., Ortiz-Rivera, W., Primera-Pedrozo, O., Hernández-Rivera, S.P. (2009). Vibrational spectroscopy standoff detection of explosives. *Anal. Bioanal. Chem.*, 395 (2), 323-335.

Perston, B.B., Hamilton, M.L., Williamson, B.E., Harland, P.W., Thomson, M.A., Melling, P.J. (2007). Grazing-Angle Fiber-Optic Fourier Transform Infrared Reflection-Absorption Spectroscopy for the in Situ Detection and Quantification of Two Active Pharmaceutical Ingredients on Glass. *Anal. Chem.*, 79, 1231-1236.

Phares, D., Holt, J., Smedley, G., Flagan, R. (2000). Method for characterization of adhesion properties of trace explosives in fingerprints and fingerprint simulations. *J. Foren. Sci.* 45 (4), 774-784.

Police: Plot to blow up aircraft failed. www.cnn.com. Posted August 10, 2006.

Primera-Pedrozo, O.M., Pacheco-Londono, L.C., De La Torre-Quintana, L.F., Hernandez-Rivera, S.P., Chamberlain, R.T., Lareau, R.T., (2004). Use of fiber optic coupled FT-IR in detection of explosives on surfaces. *Proc. SPIE Int. Soc. Opt. Eng.* 5403, 237-245.

Primera-Pedrozo, O.M., Pacheco-Londoño, L., Ruiz, O., Ramirez, M., Soto-Feliciano, Y.M., De La Torre-Quintana, L.F., Hernandez-Rivera, S.P., (2005). Characterization of thermal Inkjet technology TNT deposits by fiber optic-grazing angle probe FTIR spectroscopy. *Proc. SPIE Int. Soc. Opt. Eng.* 5778, 543-552.

Primera-Pedrozo, O.M., Rodriguez, N., Pacheco-Londono, L.C., Hernandez-Rivera, S.P., (2007). Detection of 2,4,6-trinitrotoluene on non-traditional surfaces using fiber optic coupled grazing angle probe: FTIR. *Proc. SPIE Int. Soc. Opt. Eng.*, 6542, 65423J-65410.

Primera-Pedrozo, O., Soto-Feliciano, Y., Pacheco-Londoño, L.C., Hernández-Rivera, S.P., (2008). High Explosives Mixtures Detection Using Fiber Optics Coupled: Grazing Angle Probe/Fourier Transform Reflection Absorption Infrared Spectroscopy. *Sens Imaging: Int. J.* 9 (3), 27-40

Primera-Pedrozo, O., Soto-Feliciano, Y., Pacheco-Londoño, L., Hernández-Rivera, S.P. (2009). Detection of High Explosives Using Reflection Absorption Infrared Spectroscopy with Fiber Coupled Grazing Angle Probe/FTIR. *Sens Imaging: Int. J.* 10 (1), 1-13.

Ramirez-Cedeño, M.L., Ortiz-Rivera, W., Pacheco-Londono, L C. and Hernandez- Rivera, S.P., (2010). Remote Detection of Hazardous Liquids Concealed in Glass and plastic Containers. *IEEE Sensors J.*, *10*, 693-698.

Soto-Feliciano, Y., Primera-Pedrozo, O.M., Pacheco-Londono, L., Hernandez-Rivera, S.P., (2006). Temperature dependence of detection limits of TNT on metallic surfaces using fiber optic coupled FTIR. *Proc. SPIE Int. Soc. Opt. Eng.* 6201, 62012H-62019.

Sedlacek III, A. J., Ray, M. D., Higdon, N. S. and Richter, D. A. (2001). Short-range noncontact detection of surface contamination using Raman lidar. *Proc. SPIE Int. Soc. Opt. Eng.*, *4577*, 95-104.

Sharma, S. K., Angel, S. M., Ghosh, M., Hubble, H. W. & Lucey, P. G., (2002). A remote pulsed-laser Raman spectroscopy system for mineral analysis on planetary surfaces at 66 meters. *Appl. Spectrosc*, *56*, 699-705.

Sharma, S. K., Lucey, P. G., Ghosh, M., Hubble, H. W., Horton, K. A., (2003). Stand-off Raman Spectroscopic Detection of Minerals on Planetary Surfaces. *Spectrochim. Acta A*, *59*, 2391-2407.

Sharma, S.K., Anupam, K. M. & Bhavna, S., (2005). Portable remote Raman system for monitoring hydrocarbon, gas hydrates and explosives in the environment. *Spectrochimica Acta Part A: Molecular and Biomolecular Spectroscopy,* 61, pp. 2404-2412,

Sharma, S. K., (2007). New trends in telescopic remote Raman spectroscopic instrumentation. *Spectrochim. Acta A*, *68*, 1008–1022.

Schrader, B. *Infrared and Raman spectroscopy: Methods and applications*. (1995). Schrader, B. Ed. New York, NY: VCH, p. 215.

Shimanouchi, T. (1972). Tables of Molecular Vibrational Frequencies Consolidated. vol. 1, Bethesda, MD: National Bureau of Standards.

Steinfeld, J.I.; Wormhoudt, J., (1998). *Annual Review of Physical Chemistry*, 49, 203–232

Sun, Y. and Ong, K.Y., (2005). Detection Technologies for Chemical Warfare Agents and Toxic Vapors. CRC Press, Boca Raton, FL.

Thomson, G. and Batchelder, D., (2002). Development of a hand-held forensic-lidar for standoff detection of chemicals. *Rev. Sci. Instrum.*, *73*, 4326-4328.

Umemura, J., (2002). Reflection–absorption spectroscopy of thin films on metallic substrates. In J. M. Chalmers & P. R. Griffiths, Eds., Handbook of vibrational spectroscopy. Chichester, UK: Wiley & Sons; Vol. 2, pp. 982–998.

Van Neste, C.W., Senesac, L.R., Thundat, T. (2009). Standoff Spectroscopy of Surface Adsorbed Chemicals. Analytical Chemistry, 81 (5), 1952-1956.

Wakabayashi, K., Matsumura, T., Nakayama, Y., Koshi, M., (2007). Temporal change of Raman spectra of carbon tetrachloride under laser-driven shock compression. *AIP Conference Proceedings*. 955, Issue 1, 1267-1270.

Wu, M., Ray, M., Fung, K. H., Ruckman, M. W., Harder, D. & Sedlacek III, A. J. Stand-off detection of chemicals by UV Raman spectroscopy. (2000). *Appl. Spectrosc.*, *54*, 800-806.

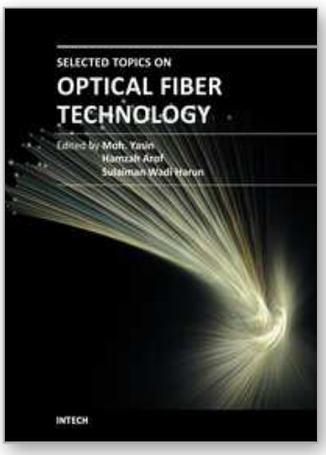

Selected Topics on Optical Fiber Technology

Edited by Dr Moh. Yasin

ISBN 978-953-51-0091-1

Hard cover, 668 pages

Publisher InTech

Published online 22, February, 2012

Published in print edition February, 2012

This book presents a comprehensive account of the recent advances and research in optical fiber technology. It covers a broad spectrum of topics in special areas of optical fiber technology. The book highlights the development of fiber lasers, optical fiber applications in medical, imaging, spectroscopy and measurement, new optical fibers and sensors. This is an essential reference for researchers working in optical fiber researches and for industrial users who need to be aware of current developments in fiber lasers, sensors and other optical fiber applications.

How to reference

In order to correctly reference this scholarly work, feel free to copy and paste the following:

Natalie Gaensbauer, Madeline Wrable-Rose, Gabriel Nieves-Colón, Migdalia Hidalgo-Santiago, Michael Ramírez, William Ortiz, Leonardo C. Pacheco-Londoño and Samuel P. Hernandez-Rivera (2012). Applications of Optical Fibers to Spectroscopy: Detection of High Explosives and Other Threat Chemicals, Selected Topics on Optical Fiber Technology, Dr Moh. Yasin (Ed.), ISBN: 978-953-51-0091-1, InTech, Available from: http://www.intechopen.com/books/selected-topics-on-optical-fiber-technology/applications-of-optical-fibers-to-spectroscopy

INTECH
open science | open minds

InTech Europe
University Campus STeP Ri
Slavka Krautzeka 83/A
51000 Rijeka, Croatia
Phone: +385 (51) 770 447
Fax: +385 (51) 686 166
www.intechopen.com

InTech China
Unit 405, Office Block, Hotel Equatorial Shanghai
No.65, Yan An Road (West), Shanghai, 200040, China
中国上海市延安西路65号上海国际贵都大饭店办公楼405单元
Phone: +86-21-62489820
Fax: +86-21-62489821

IntechOpen